

Schwinger boson symmetric spin liquids of Shastry-Sutherland model

Ke Liu

International Center for Quantum Materials, School of Physics, Peking University, Beijing 100871, China

Fa Wang*

International Center for Quantum Materials, School of Physics, Peking University, Beijing 100871, China and Collaborative Innovation Center of Quantum Matter, Beijing 100871, China

(Dated: September 1, 2023)

Motivated by recent experimental and numerical evidences of deconfined quantum critical point and quantum spin-liquid states in spin-1/2 Heisenberg model on Shastry-Sutherland lattice, we studied possible symmetric spin liquid states and their proximate ordered states under Schwinger boson formalism. We found a symmetric gapped Z_2 spin-liquid state for intermediate model parameter $0.66 < J_1/J_2 < 0.71$ under mean-field approximation. The Schwinger boson mean-field picture is partially supported by exact-diagonalization and self-consistent spin wave theory results.

I. INTRODUCTION

Recently the quasi-two-dimensional materials $S = 1/2$ quantum magnets $\text{SrCu}_2(\text{BO}_3)_2$ [1–4] attracted a lot of research interest, as they are one of the most promising realizations of deconfined quantum critical points (DQCP)[5–8] or spin-liquid states[9]. The in-plane antiferromagnetic (AFM) Heisenberg interactions between the copper atoms of $\text{SrCu}_2(\text{BO}_3)_2$ makes it a potential realization of the Shastry-Sutherland model[10] shown in Fig. 1 (a). A Néel state forms when the nearest neighbor coupling J_1 is large and a dimer valence bond solid forms when second neighbor coupling J_2 is large[10]. The issue is the intermediate phase [11–14] between the Néel phase and dimer-singlet (DS) phase [also called orthogonal dimer (OD) phase in some literature]. There are a variety of prediction of the intermediate phase by difference theories and numerics: a direct transition from dimer-singlet phase to Néel phase[15, 16], a helical order[17, 18], columnar dimers[19], or plaquette-singlet[12, 16, 18] intermediate phase. Recently there are experimental[2–4] and numerical[14, 20–23] evidences of the existence of the plaquette-singlet (PS) phase [also called plaquette singlet solid (PSS) or plaquette valence bond solid (PVBS) in some literature]. The phase transition between the Néel and plaquette-singlet phase may be described by a DQCP with emergent $O(4)$ symmetry[13, 20] and deconfined spinon excitations. And evidences of a proximate DQCP were found on the boundary of plaquette-singlet phase and Néel AFM phase in a NMR study of $\text{SrCu}_2(\text{BO}_3)_2$ under external magnetic field[1].

Some recent numerical studies including density-matrix renormalization group (DMRG)[24], exact diagonalization (ED)[25], and pseudofermion functional renormalization group[26] also suggest the existence of a spin liquid phase in a narrow range of coupling parameter J_1/J_2 between the PS phase and Néel phase without magnetic field. This intriguing possibility has not been thoroughly studied theoretically, especially using the traditional slave particle language for spin liquids[27]. With this motivation we study the possible symmetric spin-liquid states and their proximate ordered states on Shastry-Sutherland lattice under Schwinger boson formalism[28] in this paper. The goal of our work is not to accurately determine the phase diagram of the Shastry-Sutherland model, but to explore the possibilities of quantum spin liquids compatible with this lattice, which might be realized in related models and materials.

In this paper, we focus on the Schwinger boson description of quantum spin liquids, which is convenient to describe the transition between gapped Z_2 spin-liquid phases and magnetic ordered phases[29]. By projective symmetry group (PSG)[30, 31], we find 6 possible algebraic Z_2 PSG solutions and 4 gauge inequivalent ansatz. Comparing the mean-field energies of these ansatz, we find a symmetric gapped Z_2 spin liquid for the intermediate model parameter $0.66 < J_1/J_2 < 0.71$ under mean-field approximation. A dimer-singlet phase forms in $J_1/J_2 < 0.66$ while a Néel AFM state forms in $J_1/J_2 > 0.71$, where the Schwinger boson condensation happens. To further investigate the PS state, we also study ansatz with PS order, and find that these PS ansatz have higher ground state energy compared with the symmetric spin liquids in the mean-field level.

We also study the spin correlations of ground state wave function and structure factor of the spin-liquid states and Néel state by the Schwinger boson mean-field theory(SBMFT), and compare them with the results of exact-diagonalization and spin-wave theory. We find that the spin correlations in SBMFT have similar behavior compared

* wangfa@pku.edu.cn

with the result of the exact diagonalization method. The structure factor in the Néel phase can also be calculated by the spin wave theory. However, the linear spin wave theory breaks down near $J_1/J_2 \sim 1$, which is far from the Néel phase boundary. To investigate the Néel phase in $J_1/J_2 < 1$ region, we use a self-consistent spin wave theory, which pushes the Néel phase boundary down to $J_1/J_2 \approx 0.65$. With the self-consistent spin wave theory, we get qualitatively consistent dynamical spin correlations with Schwinger boson mean-field theory.

This paper is organized as follows. In Sec. II, We introduce the Shastry-Sutherland model and Schwinger boson mean-field theory, present the mean-field phase diagram with a gapped Z_2 spin liquid state in the intermediate parameter $0.66 < J_1/J_2 < 0.71$. In Sec. III, we compare the structure factors for the spin liquid and Néel states by SBMFT and self-consistent spin wave theory, and compare some of the ground state properties by SBMFT and exact diagonalization. Section IV contains further discussion and a summary of results. The technical and numerical details are presented in the Appendix.

II. SCHWINGER BOSON SYMMETRIC SPIN LIQUIDS

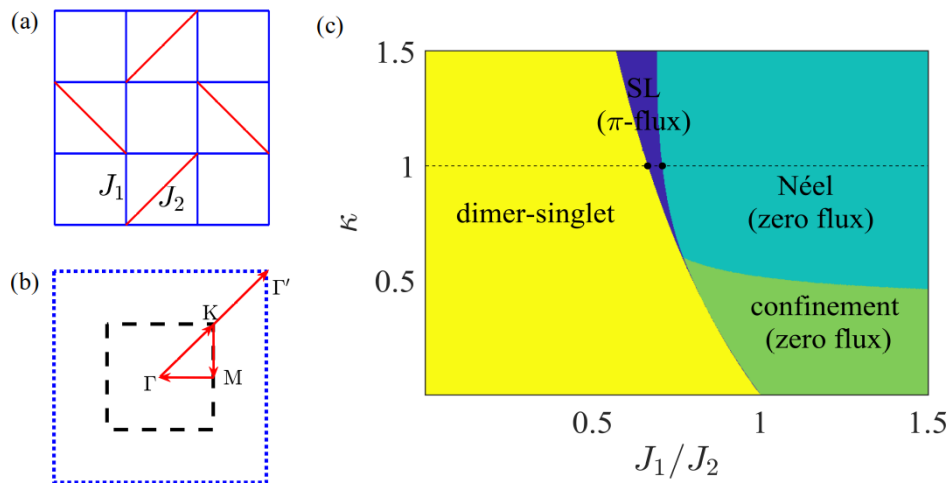


FIG. 1: (a) is the Shastry-Sutherland lattice. The Heisenberg couplings in blue and red bonds are J_1 and J_2 respectively. The black dashed line in (b) is the first Brillouin zone of Shastry-Sutherland lattice, and the blue dotted line is the first Brillouin zone of square lattice without J_2 bonds. The red arrows are the plot paths ($K \rightarrow M \rightarrow \Gamma \rightarrow K \rightarrow \Gamma'$) in this paper. (c) is the phase diagram of Schwinger boson mean-field theory for Shastry-Sutherland model. The phase boundaries at physical condition $\kappa = 1$ are $J_1/J_2 = 0.66$ and $J_1/J_2 = 0.71$. In the mean-field level, the phase transition from DS to SL is continuous while the phase transition from SL to Néel is first order.

The Shastry-Sutherland model Hamiltonian is

$$H = J_1 \sum_{\langle ij \rangle} \mathbf{S}_i \cdot \mathbf{S}_j + J_2 \sum_{\langle\langle ij \rangle\rangle'} \mathbf{S}_i \cdot \mathbf{S}_j, \quad (1)$$

where \mathbf{S}_i are $S = 1/2$ spin operators and $\langle ij \rangle$ are the nearest-neighbor[blue in Fig. 1(a)] bonds, while $\langle\langle ij \rangle\rangle'$ are some of the next-nearest-neighbor[red in Fig. 1(a)] bonds. Here we study this Hamiltonian by the Schwinger boson mean-field theory. The spin operator is expressed by the Schwinger bosons as

$$\mathbf{S}_i = \frac{1}{2} \sum_{\alpha, \beta = \uparrow, \downarrow} b_{i\alpha}^\dagger \boldsymbol{\sigma}_{\alpha\beta} b_{i\beta}, \quad (2)$$

with the constraints at every site

$$\sum_{\sigma} b_{i\sigma}^\dagger b_{i\sigma} = \kappa = 2S, \quad (3)$$

for a spin system with spin S . For the convenience of analysis, κ is usually regarded as a continuous parameter. Using the Schwinger boson representation, the Heisenberg interaction can be rewritten as

$$\mathbf{S}_i \cdot \mathbf{S}_j =: \hat{B}_{ij}^\dagger \hat{B}_{ij} : - \hat{A}_{ij}^\dagger \hat{A}_{ij} \quad (4)$$

where $::$ is normal ordering and boson pairing operator \hat{A} and hopping operator \hat{B} are defined as

$$\hat{B}_{ij} = \frac{1}{2} \sum_{\sigma} b_{i\sigma}^{\dagger} b_{j\sigma}, \quad (5)$$

$$\hat{A}_{ij} = \frac{1}{2} \sum_{\sigma, \sigma'} \epsilon_{\sigma\sigma'} b_{i\sigma} b_{j\sigma'}. \quad (6)$$

After decoupling the quartic terms by the Hubbard-Stratonovich transformation, we get the mean-field Hamiltonian:

$$H_{\text{MF}} = \sum_{ij} J_{ij} \left(-A_{ij}^* \hat{A}_{ij} + B_{ij}^* \hat{B}_{ij} + \text{H.c.} \right) + \sum_{ij} J_{ij} \left(|A_{ij}|^2 - |B_{ij}|^2 \right) - \mu_i \sum_i (\hat{n}_i - \kappa), \quad (7)$$

where the complex numbers $A_{ij} = \langle \hat{A}_{ij} \rangle = -A_{ji}$ and $B_{ij} = \langle \hat{B}_{ij} \rangle = B_{ji}^*$ are the mean-field ansatz. μ_i are the real Lagrangian multipliers to enforce the constraints of Eq. (3), which are usually site independent, namely $\mu_i = \mu$. Because of the existence of emergent $U(1)$ gauge redundancy, the mean-field solutions should be classified by projective symmetry group (PSG) [30, 31]. With the help of the PSG of Schwinger boson, we find 6 PSG solutions and 4 gauge inequivalent ansatz, which are named as (π, π) , $(0, \pi)$, $(\pi, 0)$, $(0, 0)$ -flux states according to their gauge flux distribution. The (π, π) and $(0, 0)$ -flux states are called π -flux and zero-flux hereafter. The details of the PSG solutions and ansatz are shown in Appendix.

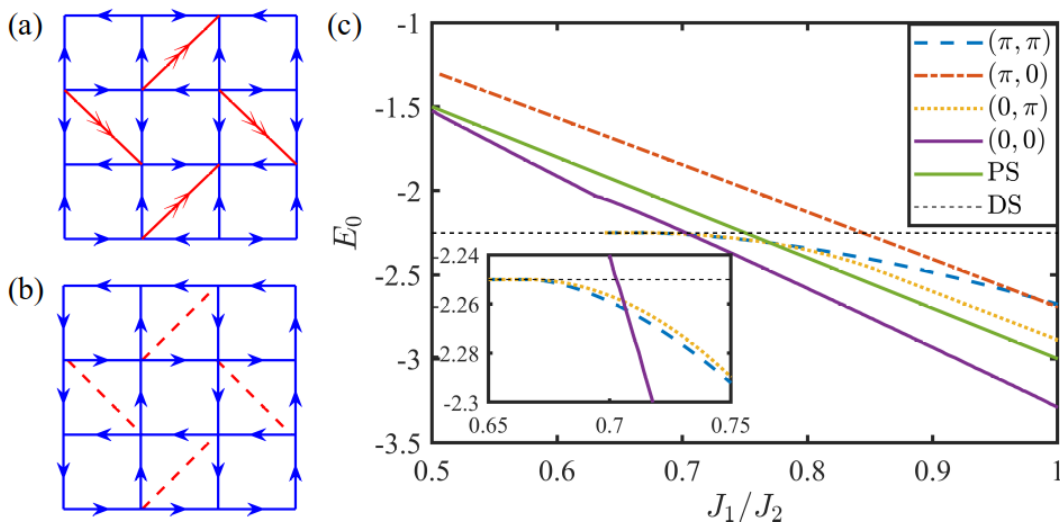


FIG. 2: (a) and (b) are the ansatz A_{ij} of the zero-flux and π -flux states respectively. An arrow from site i to j means $A_{ij} > 0$ and A_{ij} in dashed lines are zero. The different arrows represent different amplitudes of A_{ij} . (c) is the ground state energies of the 4 gauge inequivalent symmetric spin liquid ansatz and two valence bound solid (DS and PS) states. The inset in (c) is the details in $0.65 < J_1/J_2 < 0.75$. It shows that only the DS state and (π, π) -flux and $(0, 0)$ -flux SL states appear as mean-field ground states.

Comparing the mean-field ground state energies of the 4 gauge inequivalent symmetric ansatz with the change of J_1/J_2 and κ , [see Fig. 2 (c)], we get a mean-field phase diagram of the Heisenberg model in Shastry-Sutherland lattice, which is shown in Fig. 1 (c). We find only two ansatz with zero or π -flux in each plaquettes as mean-field ground states under physical condition ($\kappa = 1$). The ansatz configuration of these two state are shown in Fig. 2 (a) and (b). The π -flux state is dominant when J_2 is large and the zero-flux state is dominant when J_1 is large.

For the zero-flux mean-field state with $J_1/J_2 > 0.71$, The emergent gauge field is a staggered $U(1)$ field, and the spinons are either confined when κ is small [32] or condensed when κ is large. For physical $\kappa = 1$ the spinons of zero-flux state condense and form the Néel AFM order.

The π -flux state has Z_2 gauge field and can in principle be a stable spin liquid. It becomes the mean-field ground state for $J_1/J_2 < 0.71$, when $J_1/J_2 < 0.66$ it reduces to the confined dimer-singlet state with only $A_2 \neq 0$.

Therefore, there are three distinct phases with the change of J_1/J_2 under mean-field approximation: dimer-singlet phase for $J_1/J_2 < 0.66$, π -flux Z_2 spin liquid state for $0.66 < J_1/J_2 < 0.71$ and Néel phase for $J_1/J_2 > 0.71$. The details of PSG and mean-field solution can be referred to the Appendix.

The dynamic and static structure factors of the π -flux spin liquid state are also calculated by the Schwinger boson mean field theory and shown in Fig. 3, which may be used as numerical and experimental signatures of this spin liquid state. In particular the dominant short-range spin correlations in this π -flux SL state is related to a 4-sublattice AFM order (see Appendix).

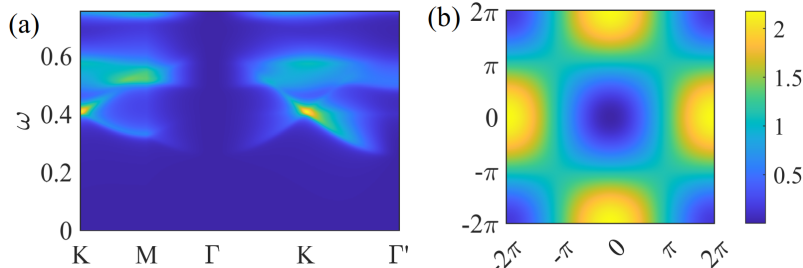


FIG. 3: (a) and (b) are the dynamic and static structure factor respectively of the π -flux Z_2 spin liquid phase. The model parameters are $J_1 = 0.7$, $J_2 = 1$. Note the plotting range of (b) is the first BZ of the square lattice without J_2 bonds.

To further investigate the PS phase, we also study mean-field ansatz with plaquette-singlet order. There are two kinds of plaquette-singlet states for the two kinds of plaquette in Shastry-Sutherland lattice. Only the mean field energy of plaquette-singlet state in the “empty” square is plotted in Fig. 2 (c), because it has lower ground state energy. The details of the plaquette-singlet state can be referred to Appendix. We find that the ground state energy of this state is always higher comparing with the minimum energy of π and zero-flux SL states with the change of parameter J_1/J_2 , which is shown in Fig. 2 (c). However, the energy differences are small near the intermediate region of parameter J_1/J_2 with π -flux SL ground state. Therefore, the PS state may emerge after considering the gauge fluctuations and projecting the mean-field wave function by Gutzwiller projection, which is beyond the scope of the current work. Because of the absence of the PS state in the mean-field level, the possible DQCP[13, 20] cannot be studied by the Schwinger boson mean field theory.

III. COMPARISON TO SELF-CONSISTENT SPIN WAVE THEORY AND ED

The Néel phase can also be studied by the spin wave theory. However, as shown in Fig. 4 (a) and (b), the linear spin wave theory breaks down at $J_1/J_2 = 1$ because the spin wave dispersion become $\epsilon_k \propto k^2$ under linear spin wave at $J_1/J_2 = 1$, and the magnetic order parameter for spin-1/2 model vanishes at $J_1/J_2 = 1.05$, which is much larger than the Néel phase boundary by other theories and numerics. The details of the spin wave dispersion can be referred to Appendix. Near the Néel phase boundary, the magnon interactions play important roles and need to be considered. However, the conventional nonlinear spin wave theory by $1/S$ expansion also breaks down near $J_1/J_2 = 1$ because the interaction correction depends on the linear spin wave Hamiltonian. Therefore, we use the self-consistent spin wave theory[33, 34] to incorporate the effects of magnon interactions. The idea of the self-consistent spin wave theory is to decouple the quartic terms of Holstein-Primakoff bosons into all possible quadratic terms, and compute these corrections to linear spin wave Hamiltonian self-consistently. The details of the self-consistent spin wave theory are given in the Appendix. The magnetic order parameter vanishes at $J_1/J_2 \approx 0.65$ by self-consistent spin wave theory as shown in Fig. 4 (b), which yields more accurate Néel phase boundary.

The dynamic structure factors in the Néel phase are calculated to compare the Schwinger boson mean-field theory and the self-consistent spin wave theory, Fig. 4 (c) and (d) are the dynamic structure factors at $J_1/J_2=0.9$ calculated by these two theories. In the Néel phase, the Schwinger boson condenses and yields sharp magnon peaks in the dynamic structure factor, while the non-condensing spinons contribute to the continuum. Although the magnon interaction is considered in the self-consistent spin wave theory, the magnon damping channel is not included. Therefore, the magnon peaks are always sharp and there is no continuum in the dynamic structure factor calculated by self-consistent spin wave theory. The dynamic structure factor calculated by self-consistent spin wave theory is more consistent with the schwinger boson mean field theory than the linear spin wave theory. We note that the energy scales of dynamic structure factors are different in the Schwinger boson mean-field theory and spin wave theory, and they should become

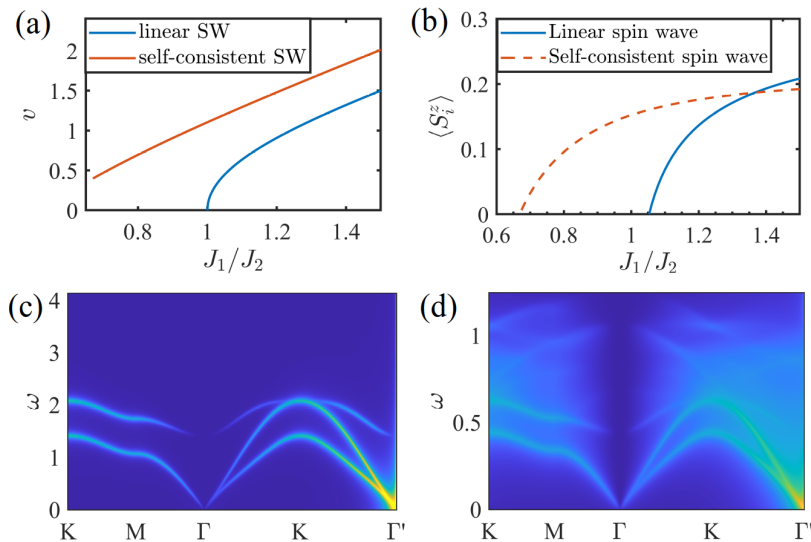


FIG. 4: (a) is the magnon velocity near the Goldstone mode calculated by linear spin wave and self-consistent spin wave theory (see Appendix). The magnon velocity of linear spin wave vanishes at $J_1/J_2 = 1$, where the magnon dispersion become $\propto k^2$ and linear spin wave theory breaks down. (b) is the Néel order parameter computed by self-consistent spin wave theory and linear spin wave theory, which vanishes at $J_1/J_2 \approx 0.65$ and $J_1/J_2 \approx 1.05$ respectively. (c) and (d) are the dynamic structure factor calculated by Schwinger boson mean-field theory and self-consistent spin wave theory in Néel phase. The parameters are $J_1 = 0.9$, $J_2 = 1$.

identical in the large S limit.

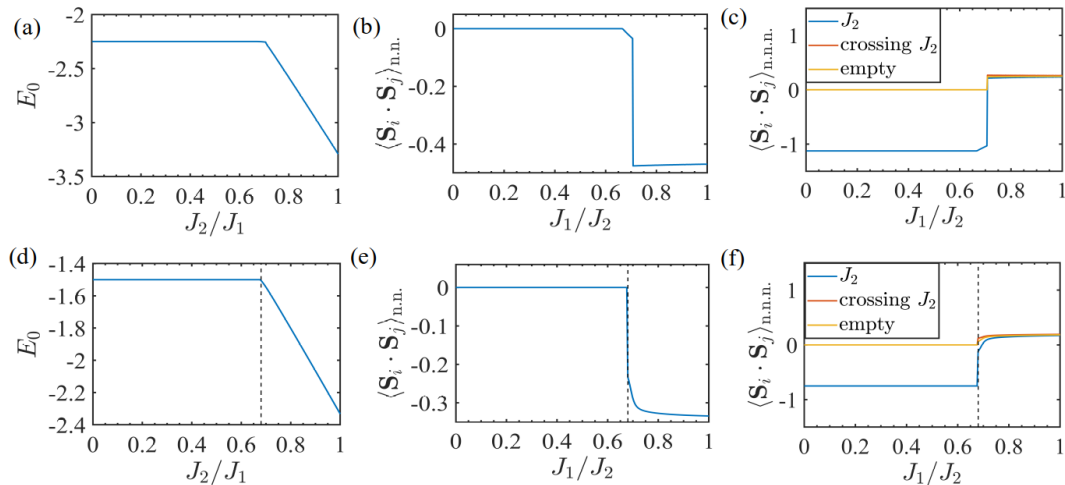


FIG. 5: (a)-(c) and (d)-(f) are observables calculated by Schwinger boson mean-field theory and 32-site exact diagonalization respectively. (a) and (d) are the ground state energy per unit cell. (b) and (e) are the nearest-neighbor (n.n.) spin correlation. (c) and (f) are the next-nearest-neighbor (n.n.n.) spin correlation. The Shastry-Sutherland lattice has three inequivalent n.n.n. bonds, which are J_2 bond, bond crossing J_2 bond, and empty bond. The dashed lines in (b), (d) and (f) are $J_1/J_2 = 0.68$.

We also compare the ground state properties computed by SBMFT and exact diagonalization. The results are shown in Fig. 5. The ground state from 32-site exact diagonalization is the exact dimer-single state for $J_1/J_2 < 0.68$, which is consistent with previous exact diagonalization studies[11, 35] and very close to the SBMFT phase boundary $J_1/J_2 \sim 0.66$ for DS phase. The near-neighbor and next-nearest-neighbor spin correlations also show similar behavior in SBMFT and exact diagonalization.

IV. DISCUSSION AND CONCLUSION

We studied the Shastry-Sutherland model by the Schwinger boson mean field theory. Using the projective symmetry group method, we find two kinds of possible symmetric ansatz. Comparing the energy of the two ansatz with the change of J_1/J_2 and κ , we get the Schwinger boson mean-field phase diagram of Shastry-Sutherland model. We find a π -flux gapped Z_2 spin liquid state for the intermediate parameter $0.66 < J_1/J_2 < 0.71$ between the dimer-singlet phase and the Néel AFM phase. This π -flux spin liquid state is continuously connected to the DS phase, but has a first-order transition to the Néel AFM phase upon increasing J_1/J_2 . The short-range spin correlations in this π -flux state is closely related to a 4-sublattice AFM order instead of Néel AFM order. We expect that ring-exchange coupling with opposite sign to that derived from the Hubbard model would further stabilize this π -flux spin liquid state[31].

To investigate the possibility of plaquette-singlet state[12, 14, 16, 18, 20–22], we studied PS ordered ansatz which break the glide symmetry. We found that the ground state energy of these PS ordered ansatz are higher compared with the symmetric spin liquid ansatz under mean-field approximation. Therefore the PS phase does not exist in our mean-field phase diagram. However the energy difference between the PS phase and spin liquids are small in the spin liquid phase. So it is possible that the PS phase may emerge after considering gauge fluctuations and Gutzwiller projection of mean-field wave functions, which we leave for future studies.

To further investigate the Néel AFM phase, we used a self-consistent spin wave theory because the linear spin wave theory breaks down for $J_1/J_2 < 1$. The self-consistent spin wave theory renormalizes the magnon dispersion by the magnon interactions, and further stabilizes the magnetic order down to $J_1/J_2 \sim 0.65$. The dynamic structure factor calculated by this theory is more consistent with the results of Schwinger boson mean-field theory except for an overall energy scale.

We have also performed exact diagonalization of the Shastry-Sutherland model with 32 sites. The results indicate that the phase boundary of dimer-singlet phase is $J_1/J_2 \sim 0.68$, which is roughly consistent with the Schwinger boson mean-field result and previous exact diagonalization studies of larger system sizes[35]. The behavior of spin correlation functions from the exact diagonalization results is similar to those of the Schwinger boson mean-field theory, which provides partial support of our mean-field picture of the Shastry-Sutherland model.

Some previous numerical studies[24–26] suggest that the spin liquid phase in Shastry-Sutherland model is gapless and possibly described by fermionic spinons with Dirac-cone dispersions similar to the DQCP[20]. This gapless spin liquid phase cannot be captured by our Schwinger boson mean-field theory. However strong interactions between fermionic spinons induced by gapless $U(1)$ gauge field might produce Cooper pairing of spinons, which may open spin gap and reduce the $U(1)$ gauge field to Z_2 . Then the gapped Z_2 fermionic spinon spin liquid is likely a dual description[36] of the Schwinger boson symmetric Z_2 spin liquids considered here. This may be an interesting direction for future theoretical and numerical studies.

V. ACKNOWLEDGEMENTS

KL thanks Fang-Yu Xiong, Xue-Mei Wang and Jie-Ran Xue for helpful discussions. FW acknowledges support from National Natural Science Foundation of China (No. 12274004), and National Natural Science Foundation of China (No. 11888101).

Appendix A: PSG classification of the symmetric spin liquid on Shastry-Sutherland lattice

The Schwinger boson mean-field theory has a emergent $U(1)$ gauge symmetry. After the local gauge transformation

$$b_{j\sigma} \rightarrow e^{i\phi(j)} b_{j\sigma}, \quad (\text{A1})$$

$$A_{ij} \rightarrow e^{i[\phi(i)+\phi(j)]} A_{ij}, \quad (\text{A2})$$

$$B_{ij} \rightarrow e^{i[-\phi(i)+\phi(j)]} B_{ij}, \quad (\text{A3})$$

the mean-field Hamiltonian is invariant and all physical observables are unchanged, as the wave function is same after projected to physical condition. Because of the existence of emergent gauge symmetry, for different spin liquids with same symmetry, the ansatz are invariant under symmetry transformations followed by gauge transformations, $\hat{b}_{\mathbf{r},s} \rightarrow \exp[i\phi_g(g\mathbf{r})]\hat{b}_{g\mathbf{r},s}$, for space group element g . Therefore, the spin-liquid states should be classified by the projective representation of the space group. The ansatz are invariant under operations of projective symmetry group (PSG). Different PSGs characterize different kinds of spin-liquid states with same symmetries.

We set up a Cartesian coordinate system and represent the site coordinate by $(x, y) = x\hat{e}_x + y\hat{e}_y$ with $x, y \in \mathbb{Z}$. For the discussion convenience, the site coordinate can also be expressed by cell-sublattice index, (X, Y, s) , where

For a defining relation $g_1 g_2 \cdots g_k = \mathbb{1}$, we have

$$\phi_{g_1 g_2 \cdots g_k}(g_1 g_2 \cdots g_k \mathbf{r}) + \phi_{g_2 \cdots g_k}(g_2 \cdots g_k \mathbf{r}) + \cdots + \phi_{g_k}(g_k \mathbf{r}) = (\text{an IGG element}) = p\pi, p \in \mathbb{Z}_2. \quad (\text{A17})$$

Note that all these equations about ϕ s are implicitly modulo 2π .

We consider a gauge transformation $\hat{b}_{\mathbf{r},s} = \exp[i\phi(\mathbf{r})]\hat{b}'_{\mathbf{r},s}$, then the generators of PSG transformed as

$$\phi'_g(g\mathbf{r}) = \phi_g(g\mathbf{r}) + \phi(g\mathbf{r}) - \phi(\mathbf{r}). \quad (\text{A18})$$

With this relation, by choosing $\phi(X, Y, s)$ for all $X \neq 0$, we can make $\phi'_{T_X}(X, Y, s) = 0$ for all X, Y, s ; then by choosing $\phi(X = 0, Y, s)$, we can make $\phi'_{T_Y}(X = 0, Y, s) = 0$ for all Y, s . we are still left three gauge freedoms. The first one is the global constant phase,

$$\phi(X, Y, s)_1 = \phi_s, \quad (\text{A19})$$

this does not change ϕ_{T_X} and ϕ_{T_Y} , but will change ϕ_{C_4} and ϕ_σ as

$$\phi'_{C_4}(X, Y, s) = \phi_{C_4}(X, Y, s) + \phi_s - \phi_{s-1}, \quad (\text{A20})$$

$$\phi'_\sigma(X, Y, s) = \phi_\sigma(X, Y, s) + \phi_s - \phi_{-s}. \quad (\text{A21})$$

The second gauge freedom is

$$\phi(X, Y, s)_2 = \pi \cdot X, \quad (\text{A22})$$

which also does not change ϕ_{T_X} and ϕ_{T_Y} modulo IGG, but will change ϕ_{C_4} and ϕ_σ as

$$\phi'_{C_4}(X, Y, s) = \phi_{C_4}(X, Y, s) + \pi \cdot (X - Y), \quad (\text{A23})$$

$$\phi'_\sigma(X, Y, s) = \phi_\sigma(X, Y, s) + \pi \cdot (X - Y - x_{-s}). \quad (\text{A24})$$

The third gauge freedom is

$$\phi(X, Y, s)_3 = \pi \cdot (X + Y), \quad (\text{A25})$$

which does not change ϕ_{T_X} and ϕ_{T_Y} and ϕ_{C_4} modulo IGG, but will change ϕ_σ as

$$\begin{aligned} \phi'_\sigma(X, Y, s) &= \phi_\sigma(X, Y, s) - \pi \cdot (x_{-s} + y_{-s}) \\ &= \phi_\sigma(X, Y, s) + \pi \cdot s. \end{aligned} \quad (\text{A26})$$

We then consider the relation of the generators of the space group. From the relation of Eq. (A8), the algebraic constraint is (ϕ_{T_X} omitted hereafter),

$$\phi_{T_Y}(X + 1, Y, s) - \phi_{T_Y}(X, Y, s) = p_1\pi, \quad (\text{A27})$$

then the solution is

$$\phi_{T_Y}(X, Y, s) = p_1\pi \cdot X. \quad (\text{A28})$$

The algebraic constraint from relation of Eq. (A9) is

$$-\phi_{T_Y}(X, Y + 1, s) + \phi_{C_4}(X + 1, Y + 1, s) - \phi_{C_4}(X, Y, s) = p_2\pi, \quad (\text{A29})$$

then we have

$$\phi_{C_4}(X + 1, Y + 1, s) - \phi_{C_4}(X, Y, s) = p_2\pi + p_1\pi \cdot X \quad (\text{A30})$$

From the relation of Eq. (A10), we have

$$\phi_{C_4}(X + 1, Y, s) - \phi_{T_Y}(Y, -X, s - 1) - \phi_{C_4}(X, Y, s) = p_3\pi, \quad (\text{A31})$$

which yields

$$\phi_{C_4}(X+1, Y, s) - \phi_{C_4}(X, Y, s) = p_3\pi + p_1\pi \cdot Y. \quad (\text{A32})$$

Combining with Eq. (A30), the solution is

$$\phi_{C_4}(X, Y, s) = \phi_{C_4}(X, Y, s) + p_2\pi \cdot Y + p_3\pi \cdot (X - Y) + p_1\pi \cdot [XY - \frac{1}{2}Y(Y+1)] \quad (\text{A33})$$

Note that we can use the gauge freedom ϕ_2 to set $p_3 = 0$.

From the relation of Eq. (A11), the algebraic constraint is

$$\phi_{C_4}(X, Y, s) + \phi_{C_4}(Y, -X, s+3) + \phi_{C_4}(-X, -Y, s+2) + \phi_{C_4}(-Y, X, s+1) = p_4\pi, \quad (\text{A34})$$

from which we have

$$\sum_s \phi_{C_4}(0, 0, s) + p_1\pi \cdot (X^2 + Y^2) = p_4\pi. \quad (\text{A35})$$

Therefore we must have $p_1 = 0$, then $\phi_{T_Y}(X, Y, s) = 0$. For simplicity, we define $\phi_{C_4,s} = \phi_{C_4}(0, 0, s)$, then we have the solution

$$\phi_{C_4}(X, Y, s) = p_2\pi \cdot Y + \phi_{C_4,s}, \quad (\text{A36})$$

with $\sum_s \phi_{C_4,s} = p_4\pi$.

The relation of Eq. (A12) yields

$$\phi_\sigma(X+1, Y, s) - \phi_{T_Y}(-Y + x_{-s}, -X + y_{-s}, -s) - \phi_\sigma(X, Y, s) = p_5\pi, \quad (\text{A37})$$

then we have

$$\phi_\sigma(X+1, Y, s) - \phi_\sigma(X, Y, s) = p_5\pi. \quad (\text{A38})$$

Then we consider the relation of Eq. (A13), which yields

$$-\phi_{T_Y}(X, Y+1, s) + \phi_\sigma(X, Y+1, s) - \phi_\sigma(X, Y, s) = p_6\pi, \quad (\text{A39})$$

then we have

$$\phi_\sigma(X, Y+1, s) - \phi_\sigma(X, Y, s) = p_6\pi. \quad (\text{A40})$$

Combined with Eq. (A38), we get the solution

$$\phi_\sigma(X, Y, s) = \phi_\sigma(0, 0, s) + p_5\pi \cdot X + p_6\pi \cdot Y. \quad (\text{A41})$$

Finally, we consider the relations of Eq. (A14) and Eq. (A15). The algebraic constraint of Eq. (A14) is

$$\phi_\sigma(X, Y, s) - \phi_\sigma(-Y - y_s, -X - x_s, -s) = p_7\pi. \quad (\text{A42})$$

Substitute Eq. (A41) to this equation, we get

$$\phi_\sigma(0, 0, s) + \phi_\sigma(0, 0, -s) + (p_5 - p_6)\pi \cdot (X - Y) - p_5\pi y_s - p_y\pi x_s = p_7\pi \quad (\text{A43})$$

then we must have $p_5 = p_6$. For simplicity, we define $\phi_{\sigma,s} = \phi_\sigma(0, 0, s)$, then $\phi_\sigma(X, Y, s) = p_5\pi \cdot (X + Y) + \phi_{\sigma,s}$, and $\phi_{\sigma,s} + \phi_{\sigma,-s} = p_7\pi + p_5\pi \cdot s$. The relation Eq. (A15) yields

$$\phi_{C_4}(X+1, Y, s) + \phi_\sigma(Y, -X-1, s-1) + \phi_{C_4}(X+x_s, -Y-y_s, 1-s) - \phi_\sigma(X, Y, s) = p_8\pi. \quad (\text{A44})$$

Substitute Eq. (A36) and (A41), we have

$$\phi_{C_4,s} + \phi_{C_4,1-s} + p_2\pi \cdot (-y_s) + \phi_{\sigma,s-1} - \phi_{\sigma,s} - p_5\pi = p_8\pi, \quad (\text{A45})$$

which yields the following 4 equations by setting the value of s ,

$$\phi_{C_4,0} + \phi_{C_4,1} + \phi_{\sigma,3} - \phi_{\sigma,0} = p_8\pi + p_5\pi \quad (\text{A46})$$

$$\phi_{C_4,1} + \phi_{C_4,0} + \phi_{\sigma,0} - \phi_{\sigma,1} = p_8\pi + p_5\pi \quad (\text{A47})$$

$$\phi_{C_4,2} + \phi_{C_4,3} + \phi_{\sigma,1} - \phi_{\sigma,2} = p_8\pi + p_5\pi + p_2\pi \quad (\text{A48})$$

$$\phi_{C_4,3} + \phi_{C_4,2} + \phi_{\sigma,2} - \phi_{\sigma,3} = p_8\pi + p_5\pi + p_2\pi \quad (\text{A49})$$

With Eq. (A46)-Eq. (A47), we get $(\phi_{\sigma,3} + \phi_{\sigma,1}) - 2\phi_{\sigma,0} = p_5\pi = 0$, then we have $p_5 = 0$. Then we can set $p_8 = 0$ by using gauge freedom ϕ_3 . With the gauge freedom ϕ_1 , we can also set $\phi_{C_4,1} = \phi_{C_4,2} = \phi_{C_4,3} = 0$, then we have $\phi_{C_4,0} = p_4\pi$. To conclude, the solutions to $\phi_{\sigma,s}$ are (modulo IGG),

$$\phi_{\sigma,0} = \frac{p_7\pi}{2} + p_4\pi, \quad (\text{A50})$$

$$\phi_{\sigma,3} = \frac{p_7\pi}{2}, \quad (\text{A51})$$

$$\phi_{\sigma,1} = \frac{p_7\pi}{2}, \quad (\text{A52})$$

$$\phi_{\sigma,2} = \frac{p_7\pi}{2} + p_2\pi. \quad (\text{A53})$$

Finally, we get the final solution to algebraic PSG:

$$\phi_{T_X}(X, Y, s) = 0, \quad (\text{A54})$$

$$\phi_{T_Y}(X, Y, s) = 0, \quad (\text{A55})$$

$$\phi_{C_4}(X, Y, s) = p_2\pi \cdot Y + p_4\pi \cdot \delta_{s,0}, \quad (\text{A56})$$

$$\phi_{\sigma}(X, Y, s) = \frac{p_7\pi}{2} + p_2\pi \cdot x_s y_s + p_4\pi \cdot \delta_{s,0}, \quad (\text{A57})$$

with three remaining free Z_2 integer parameters p_2, p_4, p_7 . Therefore, there are at most 8 kinds of PSGs.

Then we need to consider the constraints on PSG by ansatz. The nn bond poses no constraint, because there is no nontrivial space group element that maps one nn bond to itself or its reverse. For the nnn bond, if $A_{nnn} \neq 0$, consider $(0, 0, 0) - (0, -1, 2)$, which is invariant under σ , then $\phi_{\sigma}(0, 0, 0) + \phi_{\sigma}(0, -1, 2) = p_7\pi + p_2\pi + p_4\pi = 0$, namely $p_2 + p_4 + p_7 = 0$; if $B_{nnn} \neq 0$, consider $(0, 0, 0) - (0, -1, 2)$, which is invariant under σ , then $\phi_{\sigma}(0, 0, 0) - \phi_{\sigma}(0, -1, 2) = -p_2\pi - p_4\pi = 0$, namely $p_2 + p_4 = 0$, this is incompatible with $A_{nnn} \neq 0$; consider $(-1, 0, 1) - (0, 0, 3)$, which is reverted by σ , then $\phi_{\sigma}(-1, 0, 1) - \phi_{\sigma}(0, 0, 3) = 0$, then if $B_{nnn} \neq 0$, it must be real. If we only consider the condition where at least one of A_{nnn} and B_{nnn} is not zero, there are at most 6 kinds of PSGs with these constraints. If we assume the nearest-neighbor ansatz A_1 is nonzero, these 6 states can be classified by two gauge invariant phase Φ_1 and Φ_2 , which are defined on empty square plaquettes and J_2 square plaquettes respectively,

$$A_{ij}(-A_{jk}^*)A_{kl}(-A_{li}^*) = |A_1|^4 e^{i\Phi}. \quad (\text{A58})$$

We find these ansatz with same gauge flux (Φ_1, Φ_2) are gauge equivalent, therefore, we have 4 gauge inequivalent ansatz. We will show the ansatz and the properties of these 6 kinds of PSGs in the following.

2. $A_{n.n.n.} \neq 0$ and $B_{n.n.n.} = 0$

In this condition, $p_2 + p_4 = 1$ and $p_7 = 1$, and there are two possible ansatz.

For the $(p_2, p_4, p_7) = (1, 0, 1)$ condition, we have PSG solution

$$\phi_{T_x}(X, Y, s) = 0, \quad (\text{A59})$$

$$\phi_{T_y}(X, Y, s) = 0, \quad (\text{A60})$$

$$\phi_{C_4}(X, Y, s) = \pi \cdot Y, \quad (\text{A61})$$

$$\phi_{\sigma}(X, Y, s) = \frac{\pi}{2} + x_s y_s \pi, \quad (\text{A62})$$

from which we get the $(0, \pi)$ -flux ansatz in this condition, which is shown in Fig. 7. Therefore, after considering the fluctuation of gauge field and Gutzwiller projection, the $(0, \pi)$ -flux may also exist in the phase diagram.

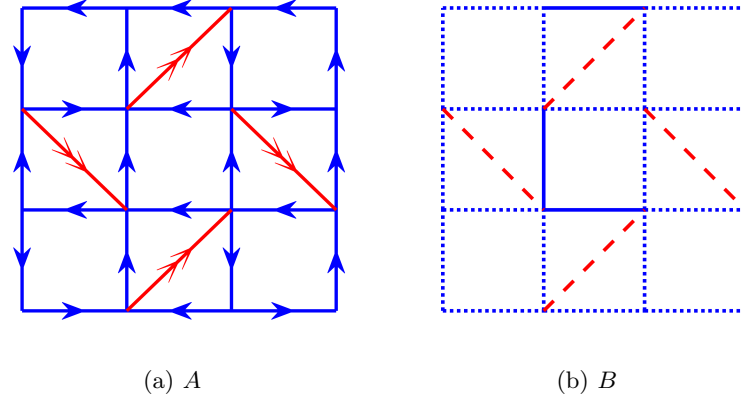


FIG. 7: The ansatz in dashed lines are 0. The ansatz B are all real and in solid and dotted lines have opposite sign. It is 0-flux in empty square and π -flux in J_2 square.

For the $(p_2, p_4, p_7) = (0, 1, 1)$ condition, we have

$$\phi_{T_x}(X, Y, s) = 0, \quad (\text{A63})$$

$$\phi_{T_y}(X, Y, s) = 0, \quad (\text{A64})$$

$$\phi_{C_4}(X, Y, s) = \delta_{s,0}\pi, \quad (\text{A65})$$

$$\phi_{\sigma}(X, Y, s) = \frac{\pi}{2} + \delta_{s,0}\pi. \quad (\text{A66})$$

The ansatz are (π, π) -flux, which is shown in Fig. 8

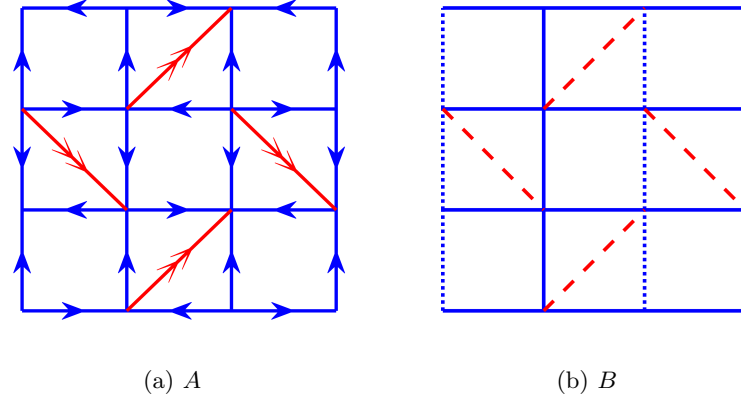


FIG. 8: The ansatz on dashed lines are 0. The ansatz B are all real and on solid and dotted lines have opposite sign. It is π -flux in empty square and π -flux in J_2 square.

3. $A_{n,n,n} = 0$ and $B_{n,n,n} \neq 0$

In this condition, $p_2 + p_4 = 0$ and there are no constraint on p_7 . Therefore, there are four types of possible ansatz. First we consider $p_2 = p_4 = 0$ condition. For $(p_2, p_4, p_7) = (0, 0, 0)$ condition, the PSG solution is

$$\phi_{C_4}(X, Y, s) = 0, \quad (\text{A67})$$

$$\phi_{\sigma}(X, Y, s) = 0. \quad (\text{A68})$$

while $(p_2, p_4, p_7) = (0, 0, 1)$ is

$$\phi_{C_4}(X, Y, s) = 0, \quad (\text{A69})$$

$$\phi_{\sigma}(X, Y, s) = \frac{\pi}{2}. \quad (\text{A70})$$

The ansatz of these two conditions are both $(0,0)$ -flux and gauge equivalent, which are shown in Fig. 9.

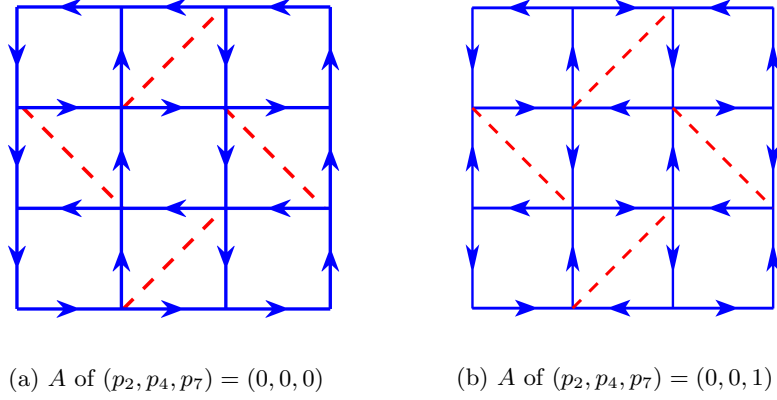


FIG. 9: The ansatz on dashed lines are 0. The two ansatz are gauge equivalent. It is 0-flux in empty square and 0-flux in J_2 square. $B_{n,n} = 0$ and $B_{n,n,n}$ are real and uniform.

Then we consider $p_2 = p_4 = 1$ condition. For $(p_2, p_4, p_7) = (1, 1, 0)$ condition, the PSG solution is

$$\phi_{C_4}(X, Y, s) = Y\pi + \delta_{s,0}, \quad (\text{A71})$$

$$\phi_{\sigma}(X, Y, s) = x_s y_s \pi + \delta_{s,0} \pi. \quad (\text{A72})$$

while $(p_2, p_4, p_7) = (1, 1, 1)$ is

$$\phi_{C_4}(X, Y, s) = Y\pi + \delta_{s,0}, \quad (\text{A73})$$

$$\phi_{\sigma}(X, Y, s) = \frac{\pi}{2} + x_s y_s \pi + \delta_{s,0} \pi. \quad (\text{A74})$$

The ansatz are both $(\pi, 0)$ -flux and also gauge equivalent.

4. Plaquette-singlet state

Now we consider the plaquette-singlet states, which break the glide symmetry and are out of the algebraic PSG solutions. After self-consistent calculation, we find that only the zero-flux plaquette-singlet ansatz can be solved self-consistently, and the self-consistent solutions are such that only the ansatz(A and B) within the selected plaquettes are nonzero. Because there are two inequivalent plaquette (empty-square and J_2 -square) in the Shastry-Sutherland lattice, there are only two inequivalent plaquette-singlet ansatz, which are shown in Fig. 10.

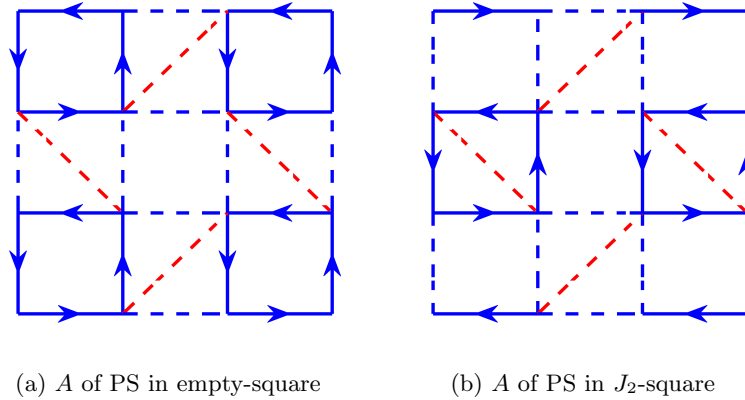


FIG. 10: The ansatz A of plaquette-singlet state in (a) empty-square and (b) J_2 -square. B of the PS state in empty-square is always zero. For the B of the PS state in J_2 -square, only the B_2 in the J_2 bonds of the J_2 -square is nonzero.

Appendix B: Mean-field theory results

In this section we will show the properties of these four gauge inequivalent spin liquid states, including the ansatz amplitudes, spinon dispersions and the spin structure factors. The static structure factor is defined as

$$S(\mathbf{k}) = \frac{1}{N_s} \sum_{i,j} \langle \mathbf{S}_i \cdot \mathbf{S}_j \rangle e^{i\mathbf{k} \cdot (\mathbf{r}_i - \mathbf{r}_j)}, \quad (\text{B1})$$

while the dynamic structure factor is

$$S(\mathbf{k}, \omega) = \frac{1}{N_s} \sum_{i,j} \langle \mathbf{S}_i(t) \cdot \mathbf{S}_j(0) \rangle e^{i\mathbf{k} \cdot (\mathbf{r}_i - \mathbf{r}_j) - i\omega t}. \quad (\text{B2})$$

In the Schwinger boson mean field theory, the structure factor can be expressed by the imaginary part of ‘‘bubble’’ Feynman diagrams. Note that the anomalous green’s function of the spinons also takes important parts. The static and dynamic spin structure factor can be measured experimentally by neutron scattering.

1. (0,0)-flux state

The mean-field Hamiltonian is shown in Eq. (7) in Main Text with the mean-field ansatz A and B shown in Fig. 9. If we choose the empty square as the unit cell, after Fourier transformation $b_{\mathbf{r}} = \frac{1}{\sqrt{N_s}} \sum_{\mathbf{k}} e^{-i\mathbf{k} \cdot \mathbf{r}} b_{\mathbf{k}}$, the mean-field Hamiltonian becomes

$$H_{\text{MF}} = \sum_{\mathbf{k}} \Psi_{\mathbf{k}}^\dagger D_{\mathbf{k}} \Psi_{\mathbf{k}} + N_s \left[\mu + \mu\kappa + 8J_1 |A_1|^2 - 2J_2 |B_2|^2 \right], \quad (\text{B3})$$

where we have used the Nambu spinor $\Psi_{\mathbf{k}} = (b_{0\mathbf{k}\uparrow}, b_{1\mathbf{k}\uparrow}, b_{2\mathbf{k}\uparrow}, b_{3\mathbf{k}\uparrow}, b_{0-\mathbf{k}\downarrow}^\dagger, b_{1-\mathbf{k}\downarrow}^\dagger, b_{2-\mathbf{k}\downarrow}^\dagger, b_{3-\mathbf{k}\downarrow}^\dagger)^T$. The subscript $s = 0, 1, 2, 3$ in $b_{s\mathbf{k}\sigma}$ is the atom index in the unit cell, which is shown in Fig. 6. The 8×8 matrix $D_{\mathbf{k}}$ satisfies

$$D_{\mathbf{k}} = -\mu \mathbf{1} + \begin{pmatrix} \mathbf{B}_{\mathbf{k}} & \mathbf{A}_{\mathbf{k}} \\ \mathbf{A}_{\mathbf{k}}^\dagger & \mathbf{B}_{-\mathbf{k}}^T \end{pmatrix}, \quad (\text{B4})$$

where $\mathbf{1}$ is the 8×8 identity matrix, and $\mathbf{A}_{\mathbf{k}}$ and $\mathbf{B}_{\mathbf{k}}$ are

$$\mathbf{A}_{\mathbf{k}} = \begin{pmatrix} 0 & \frac{1}{2} J_1 A_1 (-1 + e^{-ik_1}) & 0 & \frac{1}{2} J_1 A_1 (1 - e^{-ik_2}) \\ \frac{1}{2} J_1 A_1 (1 - e^{ik_1}) & 0 & \frac{1}{2} J_1 A_1 (-1 + e^{-ik_2}) & 0 \\ 0 & \frac{1}{2} J_1 A_1 (1 - e^{ik_2}) & 0 & \frac{1}{2} J_1 A_1 (-1 + e^{ik_1}) \\ \frac{1}{2} J_1 A_1 (-1 + e^{ik_2}) & 0 & \frac{1}{2} J_1 A_1 (1 - e^{-ik_1}) & 0 \end{pmatrix}, \quad (\text{B5})$$

$$\mathbf{B}_{\mathbf{k}} = \begin{pmatrix} 0 & 0 & \frac{1}{2} J_2 B_2 e^{-ik_2} & 0 \\ 0 & 0 & 0 & \frac{1}{2} J_2 B_2 e^{ik_1} \\ \frac{1}{2} J_2 B_2 e^{ik_2} & 0 & 0 & 0 \\ 0 & \frac{1}{2} J_2 B_2 e^{-ik_1} & 0 & 0 \end{pmatrix}. \quad (\text{B6})$$

After a Bogoliubov transformation, the mean-field Hamiltonian can be diagonalized as

$$H_{\text{MF}} = \sum_{\mathbf{k}s} \omega_{s\mathbf{k}} (\gamma_{s\mathbf{k}\uparrow}^\dagger \gamma_{s\mathbf{k}\uparrow} + \gamma_{s\mathbf{k}\downarrow}^\dagger \gamma_{s\mathbf{k}\downarrow} + 1) + N_s \left[\mu + \mu\kappa + 8J_1 |A_1|^2 - 2J_2 |B_2|^2 \right], \quad (\text{B7})$$

where the $\omega_{s\mathbf{k}}$ is the spinon dispersions, and $s = 0, 1, 2, 3$. The self-consistent equations are

$$16J_1 A_1 = - \sum_s \int_{BZ} \frac{\partial \omega_{s\mathbf{k}}}{\partial A_1} \mathbf{d}^2 k, \quad (\text{B8})$$

$$4J_2 B_2 = \sum_s \int_{BZ} \frac{\partial \omega_{s\mathbf{k}}}{\partial B_2} \mathbf{d}^2 k, \quad (\text{B9})$$

$$1 + \kappa = - \sum_s \int_{BZ} \frac{\partial \omega_{s\mathbf{k}}}{\partial \mu} \mathbf{d}^2 k, \quad (\text{B10})$$

where the integral is over the BZ. With these self-consistent equations, the mean-field ansatz can be solved. The spinon dispersion at critical spinon density κ_c and the ansatz amplitudes and are shown in Fig. 11.

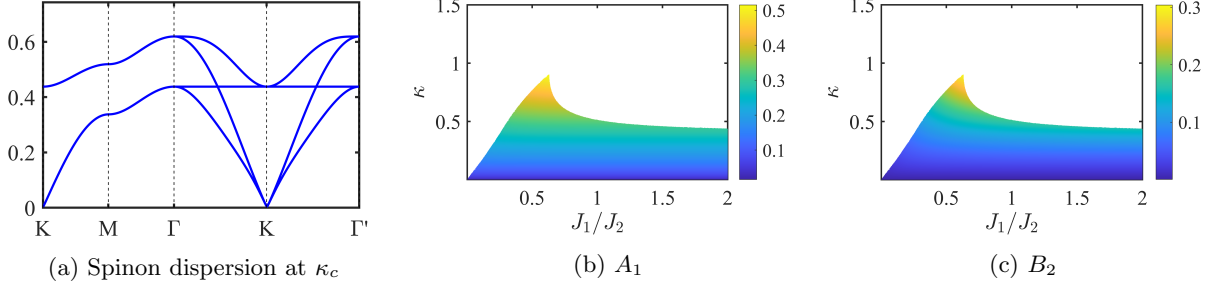


FIG. 11: (a) is the spinon dispersion at $\kappa = \kappa_c$ and $J_1 = J_2 = 1$ of (0,0)-flux state. The plot path is shown in Fig. 1 (b) in Main Text. (b) and (c) are the ansatz A_1 and B_2 value respectively. A_2 and B_1 are always zero in these two conditions. The spinon condenses at the white area in (b) and (c).

As shown in Fig.11 (a), the minima of the spinon dispersion is located at $\mathbf{Q} = (\pi, \pi)$, and vanishes at $\kappa = \kappa_c$. When κ is larger than κ_c , the spinon will condense and form a magnetic order. The spinon condenses at the white area in Fig. 11 and the contour of the ansatz amplitudes indicate the critical κ_c . We find that κ_c is always smaller than 1, therefore, the (0,0)-flux state contributes to the magnetic ordered state in the physical condition. In the condition $\kappa < \kappa_c$, the IGG of this state is $U(1)$, and this state can not exist stably.

2. $(0, \pi)$ -flux state

The mean-field Hamiltonian after Fourier transformation is

$$H_{\text{MF}} = \sum_{\mathbf{k}} \Psi_{\mathbf{k}}^\dagger D_{\mathbf{k}} \Psi_{\mathbf{k}} + N_s \left[\mu + \mu\kappa + 8J_1(|A_1|^2 - |B_1|^2) + 2J_2|A_2|^2 \right], \quad (\text{B11})$$

where

$$D_{\mathbf{k}} = -\mu\mathbf{1} + \begin{pmatrix} \mathbf{B}_{\mathbf{k}} & \mathbf{A}_{\mathbf{k}} \\ \mathbf{A}_{\mathbf{k}}^\dagger & \mathbf{B}_{-\mathbf{k}}^T \end{pmatrix}, \quad (\text{B12})$$

and

$$\mathbf{A}_{\mathbf{k}} = \begin{pmatrix} 0 & \frac{1}{2}J_1A_1(-1 - e^{-ik_1}) & -\frac{1}{2}J_2A_2e^{-ik_2} & \frac{1}{2}J_1A_1(1 + e^{-ik_2}) \\ \frac{1}{2}J_1A_1(1 + e^{ik_1}) & 0 & \frac{1}{2}J_1A_1(-1 + e^{-ik_2}) & -\frac{1}{2}J_2A_2e^{ik_1} \\ \frac{1}{2}J_2A_2e^{ik_2} & \frac{1}{2}J_1A_1(1 - e^{ik_2}) & 0 & \frac{1}{2}J_1A_1(-1 + e^{ik_1}) \\ \frac{1}{2}J_1A_1(-1 - e^{ik_2}) & \frac{1}{2}J_2A_2e^{-ik_1} & \frac{1}{2}J_1A_1(1 - e^{-ik_1}) & 0 \end{pmatrix}, \quad (\text{B13})$$

$$\mathbf{B}_{\mathbf{k}} = \begin{pmatrix} 0 & \frac{1}{2}0(-1 - e^{-ik_1}) & 0 & \frac{1}{2}0(-1 - e^{-ik_2}) \\ \frac{1}{2}0(-1 - e^{ik_1}) & 0 & \frac{1}{2}0(-1 + e^{-ik_2}) & 0 \\ 0 & \frac{1}{2}0(-1 + e^{ik_2}) & 0 & \frac{1}{2}0(-1 + e^{ik_1}) \\ \frac{1}{2}0(-1 - e^{ik_2}) & 0 & \frac{1}{2}0(-1 + e^{-ik_1}) & 0 \end{pmatrix}. \quad (\text{B14})$$

And we have also used the Nambu spinor $\Psi_{\mathbf{k}} = (b_{0\mathbf{k}\uparrow}, b_{1\mathbf{k}\uparrow}, b_{2\mathbf{k}\uparrow}, b_{3\mathbf{k}\uparrow}, b_{0-\mathbf{k}\downarrow}^\dagger, b_{1-\mathbf{k}\downarrow}^\dagger, b_{2-\mathbf{k}\downarrow}^\dagger, b_{3-\mathbf{k}\downarrow}^\dagger)^T$. The Hamiltonian can be diagonalized by a Bogoliubov transformation, which yields

$$H_{\text{MF}} = \sum_{\mathbf{k}s} \omega_{s\mathbf{k}} (\gamma_{s\mathbf{k}\uparrow}^\dagger \gamma_{s\mathbf{k}\uparrow} + \gamma_{s\mathbf{k}\downarrow}^\dagger \gamma_{s\mathbf{k}\downarrow} + 1) + N_s \left[\mu + \mu\kappa + 8J_1(|A_1|^2 - |B_1|^2) + 2J_2|A_2|^2 \right], \quad (\text{B15})$$

and the self-consistent equations are

$$16J_1A_1 = -\sum_s \int_{BZ} \frac{\partial \omega_{s\mathbf{k}}}{\partial A_1} \mathbf{d}^2k, \quad (\text{B16})$$

$$4J_2A_2 = -\sum_s \int_{BZ} \frac{\partial \omega_{s\mathbf{k}}}{\partial A_2} \mathbf{d}^2k, \quad (\text{B17})$$

$$16J_1B_1 = -\sum_s \int_{BZ} \frac{\partial \omega_{s\mathbf{k}}}{\partial B_1} \mathbf{d}^2k, \quad (\text{B18})$$

$$1 + \kappa = -\sum_s \int_{BZ} \frac{\partial \omega_{s\mathbf{k}}}{\partial \mu} \mathbf{d}^2k, \quad (\text{B19})$$

Solving these self-consistent equations we have get the ansatz amplitudes, which are shown in Fig. 7.

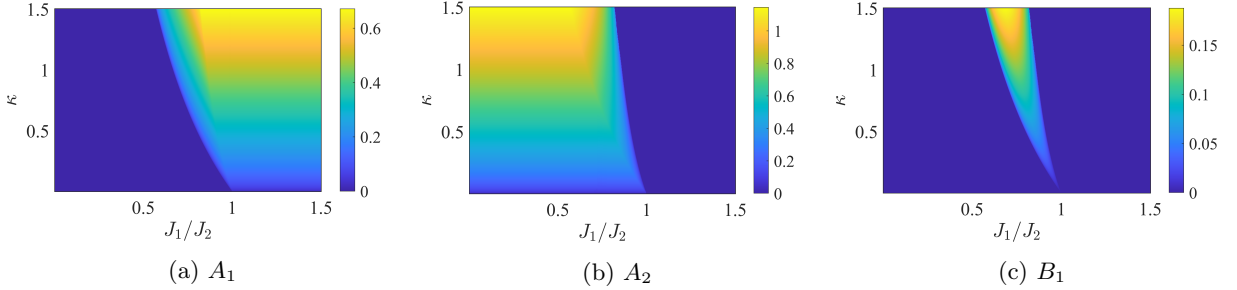


FIG. 12: The ansatz value (a) A_1 , (b) A_2 and (c) A_3 of (π, π) -flux. A_1 is finite at J_1 is large and A_2 is large at J_1 is large. B_1 is finite only when A_1 and A_2 are both finite. B_2 is always zero in this condition.

With these ansatz values, the spinon dispersion and the structure factor can be obtained, which are shown in Fig. 13. We find the bottom branch of the spinon dispersion is flat, therefore, the critical spinon density κ_c is large in this state.

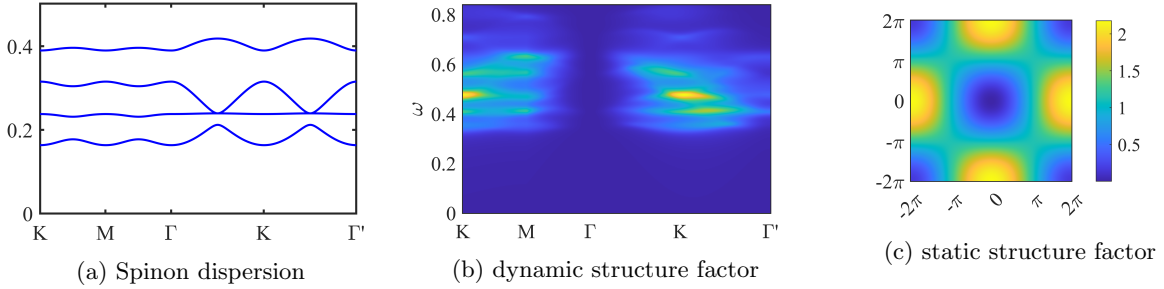


FIG. 13: (a) is the spinon dispersion, (b) is the dynamic structure factor, and (c) is the static structure factor of $(0, \pi)$ -flux state ($J_1/J_2 = 0.7$). The plot path of (a) and (b) is shown in Fig. 1 (b) in Main Text.

The ground state energy of this state is slightly higher than the energy minimum of π -flux (π, π) -flux and zero-flux $((0,0)$ -flux) state as shown in Fig. (2)(c) in Main Text, therefore, this state is not shown in the phase diagram in Fig. 1 (c) in Main Text. However, the energy difference of (π, π) and $(0, \pi)$ -flux state is very small. Therefore, this state may also exist beyond the mean-field level.

3. $(\pi, 0)$ -flux state

The mean-field Hamiltonian of the $(\pi, 0)$ -flux state in the momentum space is

$$H_{\text{MF}} = \sum_{\mathbf{k}} \Psi_{\mathbf{k}}^\dagger D_{\mathbf{k}} \Psi_{\mathbf{k}} + N_s \left[\mu + \mu\kappa + 8J_1 |A_1|^2 - 2J_2 |B_2|^2 \right], \quad (\text{B20})$$

where

$$D_{\mathbf{k}} = -\mu \mathbf{1} + \begin{pmatrix} \mathbf{B}_{\mathbf{k}} & \mathbf{A}_{\mathbf{k}} \\ \mathbf{A}_{\mathbf{k}}^\dagger & \mathbf{B}_{-\mathbf{k}}^T \end{pmatrix}, \quad (\text{B21})$$

and

$$\mathbf{A}_{\mathbf{k}} = \begin{pmatrix} 0 & \frac{1}{2}J_1A_1(-1 - e^{-ik_1}) & 0 & \frac{1}{2}J_1A_1(-1 - e^{-ik_2}) \\ \frac{1}{2}J_1A_1(1 + e^{ik_1}) & 0 & \frac{1}{2}J_1A_1(-1 + e^{-ik_2}) & 0 \\ 0 & \frac{1}{2}J_1A_1(1 - e^{ik_2}) & 0 & \frac{1}{2}J_1A_1(-1 + e^{ik_1}) \\ \frac{1}{2}J_1A_1(1 + e^{ik_2}) & 0 & \frac{1}{2}J_1A_1(1 - e^{-ik_1}) & 0 \end{pmatrix}, \quad (\text{B22})$$

$$\mathbf{B}_{\mathbf{k}} = \begin{pmatrix} 0 & 0 & \frac{1}{2}J_2B_2e^{-ik_2} & 0 \\ 0 & 0 & 0 & \frac{1}{2}J_2B_2e^{ik_1} \\ \frac{1}{2}J_2B_2e^{ik_2} & 0 & 0 & 0 \\ 0 & \frac{1}{2}J_2B_2e^{-ik_1} & 0 & 0 \end{pmatrix}. \quad (\text{B23})$$

And we have also used the Nambu spinor $\Psi_{\mathbf{k}} = (b_{0\mathbf{k}\uparrow}, b_{1\mathbf{k}\uparrow}, b_{2\mathbf{k}\uparrow}, b_{3\mathbf{k}\uparrow}, b_{0-\mathbf{k}\downarrow}^\dagger, b_{1-\mathbf{k}\downarrow}^\dagger, b_{2-\mathbf{k}\downarrow}^\dagger, b_{3-\mathbf{k}\downarrow}^\dagger)^T$. After a Bogoliubov transformation, the mean-field Hamiltonian is diagonalized as

$$H_{\text{MF}} = \sum_{\mathbf{k}s} \omega_{s\mathbf{k}} (\gamma_{s\mathbf{k}\uparrow}^\dagger \gamma_{s\mathbf{k}\uparrow} + \gamma_{s\mathbf{k}\downarrow}^\dagger \gamma_{s\mathbf{k}\downarrow} + 1) + N_s \left[\mu + \mu\kappa + 8J_1 |A_1|^2 - 2J_2 |B_2|^2 \right], \quad (\text{B24})$$

where the $\omega_{s\mathbf{k}}$ is the spinon dispersions, and $s = 0, 1, 2, 3$. The self-consistent equations are

$$16J_1A_1 = -\sum_s \int_{BZ} \frac{\partial \omega_{s\mathbf{k}}}{\partial A_1} \mathbf{d}^2k, \quad (\text{B25})$$

$$4J_2B_2 = \sum_s \int_{BZ} \frac{\partial \omega_{s\mathbf{k}}}{\partial B_2} \mathbf{d}^2k, \quad (\text{B26})$$

$$1 + \kappa = -\sum_s \int_{BZ} \frac{\partial \omega_{s\mathbf{k}}}{\partial \mu} \mathbf{d}^2k. \quad (\text{B27})$$

With these self-consistent equations, the mean-field ansatz can be solved. The spinon dispersion at physical condition $\kappa = 1$ and the ansatz amplitudes are shown in Fig. 14.

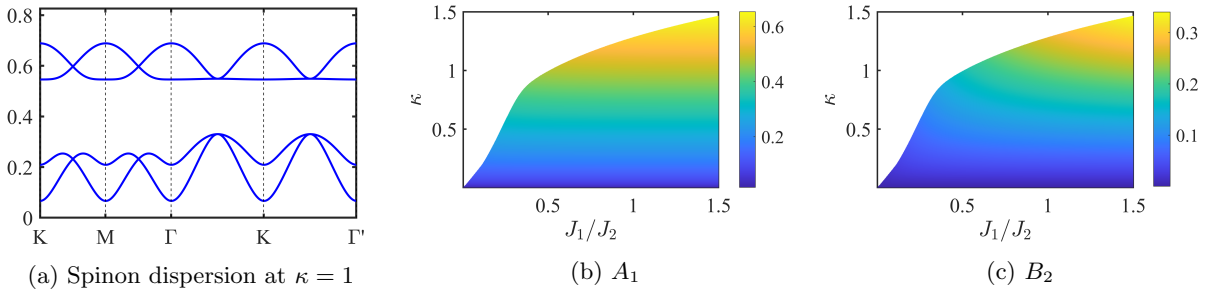


FIG. 14: (a) is the spinon dispersion at $\kappa = \kappa_c$ and $J_1 = J_2 = 1$ of $(\pi, 0)$ -flux. The plot path is shown in Fig. 1 (b) in Main Text. (b) and (c) are the ansatz A_1 and B_2 value respectively. A_2 and B_1 are always zero in this condition.

As shown in Fig. 2 (c) in the Main Text, the ground state energy of this $(\pi, 0)$ -flux is much larger than the $(0, 0)$ -flux, which may not exist even beyond the mean field level.

4. (π, π) -flux state

The mean-field Hamiltonian after Fourier transformation is

$$H_{\text{MF}} = \sum_{\mathbf{k}} \Psi_{\mathbf{k}}^\dagger D_{\mathbf{k}} \Psi_{\mathbf{k}} + N_s \left[\mu + \mu\kappa + 8J_1 (|A_1|^2 - |B_1|^2) + 2J_2 |A_2|^2 \right], \quad (\text{B28})$$

where

$$D_{\mathbf{k}} = -\mu \mathbf{1} + \begin{pmatrix} \mathbf{B}_{\mathbf{k}} & \mathbf{A}_{\mathbf{k}} \\ \mathbf{A}_{\mathbf{k}}^\dagger & \mathbf{B}_{-\mathbf{k}}^T \end{pmatrix}, \quad (\text{B29})$$

and

$$\mathbf{A}_{\mathbf{k}} = \begin{pmatrix} 0 & \frac{1}{2}J_1A_1(-1 - e^{-ik_1}) & -\frac{1}{2}J_2A_2e^{-ik_2} & \frac{1}{2}J_1A_1(-1 - e^{-ik_2}) \\ \frac{1}{2}J_1A_1(1 + e^{ik_1}) & 0 & \frac{1}{2}J_1A_1(-1 - e^{-ik_2}) & -\frac{1}{2}J_2A_2e^{ik_1} \\ \frac{1}{2}J_2A_2e^{ik_2} & \frac{1}{2}J_1A_1(1 + e^{ik_2}) & 0 & \frac{1}{2}J_1A_1(-1 - e^{-ik_1}) \\ \frac{1}{2}J_1A_1(1 + e^{ik_2}) & \frac{1}{2}J_2A_2e^{-ik_1} & \frac{1}{2}J_1A_1(1 + e^{-ik_1}) & 0 \end{pmatrix}, \quad (\text{B30})$$

$$\mathbf{B}_{\mathbf{k}} = \begin{pmatrix} 0 & \frac{1}{2}0(1 + e^{-ik_1}) & 0 & \frac{1}{2}0(-1 - e^{-ik_2}) \\ \frac{1}{2}0(1 + e^{ik_1}) & 0 & \frac{1}{2}0(1 + e^{-ik_2}) & 0 \\ 0 & \frac{1}{2}0(1 + e^{ik_2}) & 0 & \frac{1}{2}0(1 + e^{ik_1}) \\ \frac{1}{2}0(-1 - e^{ik_2}) & 0 & \frac{1}{2}0(1 + e^{-ik_1}) & 0 \end{pmatrix}. \quad (\text{B31})$$

And we have also used the Nambu spinor $\Psi_{\mathbf{k}} = (b_{0\mathbf{k}\uparrow}, b_{1\mathbf{k}\uparrow}, b_{2\mathbf{k}\uparrow}, b_{3\mathbf{k}\uparrow}, b_{0-\mathbf{k}\downarrow}^\dagger, b_{1-\mathbf{k}\downarrow}^\dagger, b_{2-\mathbf{k}\downarrow}^\dagger, b_{3-\mathbf{k}\downarrow}^\dagger)^T$. The Hamiltonian can be diagonalized by a Bogoliubov transformation, which yields

$$H_{\text{MF}} = \sum_{\mathbf{k}s} \omega_{s\mathbf{k}} (\gamma_{s\mathbf{k}\uparrow}^\dagger \gamma_{s\mathbf{k}\uparrow} + \gamma_{s\mathbf{k}\downarrow}^\dagger \gamma_{s\mathbf{k}\downarrow} + 1) + N_s \left[\mu + \mu\kappa + 8J_1(|A_1|^2 - |B_1|^2) + 2J_2|A_2|^2 \right], \quad (\text{B32})$$

and the self-consistent equations are

$$16J_1A_1 = - \sum_s \int_{BZ} \frac{\partial \omega_{s\mathbf{k}}}{\partial A_1} \mathbf{d}^2k, \quad (\text{B33})$$

$$4J_2A_2 = - \sum_s \int_{BZ} \frac{\partial \omega_{s\mathbf{k}}}{\partial A_2} \mathbf{d}^2k, \quad (\text{B34})$$

$$16J_1B_1 = - \sum_s \int_{BZ} \frac{\partial \omega_{s\mathbf{k}}}{\partial B_1} \mathbf{d}^2k, \quad (\text{B35})$$

$$1 + \kappa = - \sum_s \int_{BZ} \frac{\partial \omega_{s\mathbf{k}}}{\partial \mu} \mathbf{d}^2k, \quad (\text{B36})$$

Solving these self-consistent equations we have get the ansatz amplitudes, which are shown in Fig. 15.

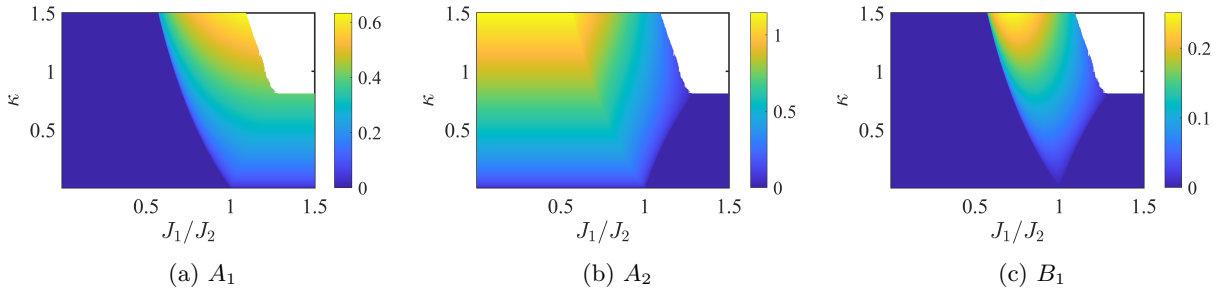


FIG. 15: The ansatz value (a) A_1 , (b) A_2 and (c) A_3 of (π, π) -flux. A_1 is finite at J_1 is large and A_2 is large at J_1 is large. B_1 is finite only when A_1 and A_2 are both finite. B_2 is always zero in this condition.

With these ansatz values, the spinon dispersion and the structure factor can be obtained, which are shown in Fig. 16.

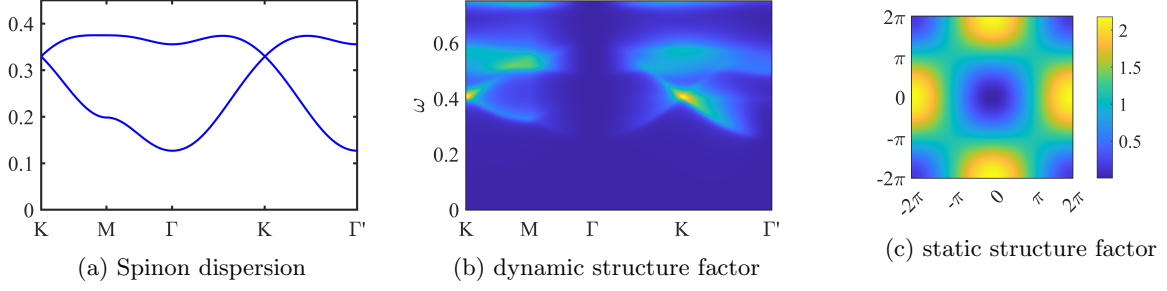


FIG. 16: (a) is the spinon dispersion, (b) is the dynamic structure factor, and (c) is the static structure factor of (π, π) -flux state ($J_1/J_2 = 0.7$). The plot path of (a) and (b) is shown in Fig. 1 (b) in Main Text.

As shown in Fig. 16 (a), the minima of the spinon dispersion is located at $\mathbf{Q} = (0, 0)$, and magnetic order will form when $\kappa > \kappa_c$.

5. Plaquette-singlet states

First we consider the plaquette-singlet state in the empty square. The mean-field Hamiltonian can be written as

$$H_{\text{MF}} = -N_s J_1 \sum_s A_1 \hat{A}_{s,s+1} + 4N_s J_1 \sum_s |A_{ij}|^2 - 4N_s \mu (\hat{n} - \kappa). \quad (\text{B37})$$

After Bogoliubov transformation, the mean-field Hamiltonian is diagonalized as

$$H_{\text{MF}} = N_s \sum_s \omega_s (\gamma_{s\uparrow}^\dagger \gamma_{s\uparrow} + \gamma_{s\downarrow}^\dagger \gamma_{s\downarrow} + 1) + N_s \left[\mu + \mu\kappa + 4J_1 |A_1|^2 \right], \quad (\text{B38})$$

and the self-consistent equations are

$$8J_1 A_1 = - \sum_s \frac{\partial \omega_s}{\partial A_1}, \quad (\text{B39})$$

$$1 + \kappa = - \sum_s \frac{\partial \omega_s}{\partial \mu}. \quad (\text{B40})$$

The mean-field Hamiltonian and the self-consistent equations of the plaquette-singlet state in J_2 -square is similar as the empty-square condition, except the existence of the B_2 in the J_2 bond. Solving the self-consistent equations, we get the ground state energies of these two plaquette-singlet states in physical condition $\kappa = 1$, which is shown in Fig. 17.

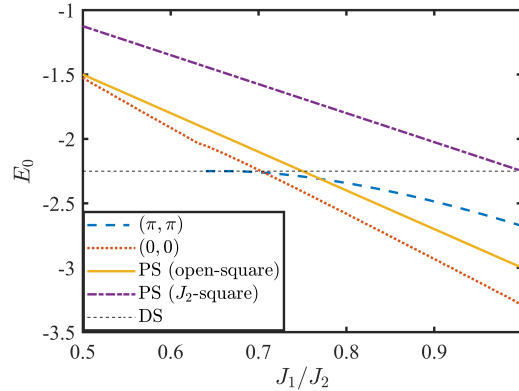


FIG. 17: The mean-field ground state energies in the physical condition $\kappa = 1$. The ground state energy of plaquette-singlet (PS) in the J_2 -square is much larger than that in the empty-square condition because of the existence of B_2 .

Appendix C: Magnetic order from the zero-flux state

In the Schwinger boson formalism, the magnetic order is formed by the condensation of the Schwinger bosons. When the density of the boson is large than the critical κ_c , the dispersion of the spinon will become zero at several \mathbf{Q} points, and the spinon will condense at these \mathbf{Q} points and develop magnetic orders.

For the Shastry-Sutherland model, the Néel phase is formed by the condensation of the zero-flux ((0,0)-flux) state. As shown in Fig. 11 (a), the dispersion of spinon become zero at $\mathbf{Q} = (\pi, \pi)$. Note that $\mathbf{Q} = -\mathbf{Q}$. If we choose the empty square as the unit cell, after Fourier transformation $b_{\mathbf{r}} = \frac{1}{\sqrt{N_s}} \sum_{\mathbf{k}} e^{-i\mathbf{k}\cdot\mathbf{r}} b_{\mathbf{k}}$, the mean-field Hamiltonian becomes

$$H_{\text{MF}} = \sum_{\mathbf{k}} \Psi_{\mathbf{k}}^\dagger D_{\mathbf{k}} \Psi_{\mathbf{k}} + N_s \left[\mu + \mu\kappa + 8J_1 |A_1|^2 - 2J_2 |B_2|^2 \right]. \quad (\text{C1})$$

where we have used the Nambu spinor $\Psi_{\mathbf{k}} = (b_{0\mathbf{k}\uparrow}, b_{1\mathbf{k}\uparrow}, b_{2\mathbf{k}\uparrow}, b_{3\mathbf{k}\uparrow}, b_{0-\mathbf{k}\downarrow}^\dagger, b_{1-\mathbf{k}\downarrow}^\dagger, b_{2-\mathbf{k}\downarrow}^\dagger, b_{3-\mathbf{k}\downarrow}^\dagger)^T$. The subscript $s = 0, 1, 2, 3$ in $b_{s\mathbf{k}\sigma}$ is the atom index in the unit cell, which is shown in Fig. 6. The 8×8 matrix $D_{\mathbf{k}}$ at \mathbf{Q} is

$$D_{\mathbf{Q}} = \begin{pmatrix} -\mu & 0 & J_2 B_2 & 0 & 0 & J_1 A_1 & 0 & J_1 A_1 \\ 0 & -\mu & 0 & J_2 B_2 & -J_1 A_1 & 0 & -J_1 A_1 & 0 \\ J_2 B_2 & 0 & -\mu & 0 & 0 & J_1 A_1 & 0 & J_1 A_1 \\ 0 & J_2 B_2 & 0 & -\mu & -J_1 A_1 & 0 & -J_1 A_1 & 0 \\ 0 & -J_1 A_1 & 0 & -J_1 A_1 & -\mu & 0 & J_2 B_2 & 0 \\ J_1 A_1 & 0 & J_1 A_1 & 0 & 0 & -\mu & 0 & J_2 B_2 \\ 0 & -J_1 A_1 & 0 & -J_1 A_1 & J_2 B_2 & 0 & -\mu & 0 \\ J_1 A_1 & 0 & J_1 A_1 & 0 & 0 & J_2 B_2 & 0 & -\mu \end{pmatrix}, \quad (\text{C2})$$

In the critical density κ_c , it satisfies

$$-\mu + J_2 B_2 - 2A_1 = 0. \quad (\text{C3})$$

At this point, $D_{\mathbf{Q}}$ has two eigenvectors with zero eigenvalue,

$$\begin{aligned} \Psi_1 &= \frac{1}{\sqrt{2}} (0 \ 1 \ 0 \ 1 \ 1 \ 0 \ 1 \ 0)^T, \\ \Psi_2 &= \frac{1}{\sqrt{2}} (-1 \ 0 \ -1 \ 0 \ 0 \ 1 \ 0 \ 1)^T. \end{aligned} \quad (\text{C4})$$

Therefore, the condensation at \mathbf{Q} is $\langle \Psi_{\mathbf{Q}} \rangle = c_1 \Psi_1 + c_2 \Psi_2$, where $c_{1,2}$ are two complex numbers. We define $x_s \equiv (\langle b_{(X,Y,s)\uparrow} \rangle, \langle b_{(X,Y,s)\downarrow} \rangle)^T$, then condensation on site (X, Y, s) is given by

$$\begin{aligned} x_0 &= x_2 = \frac{(-1)^{X+Y}}{\sqrt{2}} \begin{pmatrix} -c_2 \\ c_1^* \end{pmatrix}, \\ x_1 &= x_3 = \frac{(-1)^{X+Y}}{\sqrt{2}} \begin{pmatrix} c_1 \\ c_2^* \end{pmatrix}, \end{aligned} \quad (\text{C5})$$

and the ordered magnetic momentum is then $\mathbf{S}(X, Y, s) = \frac{1}{2} x_s^\dagger \boldsymbol{\sigma} x_s$. Thus we have

$$\mathbf{S}(X, Y, 0) = \mathbf{S}(X, Y, 2) = \mathbf{n}, \quad (\text{C6})$$

$$\mathbf{S}(X, Y, 1) = \mathbf{S}(X, Y, 3) = -\mathbf{n}, \quad (\text{C7})$$

where \mathbf{n} is the $SO(3)$ vector corresponded with the $SU(2)$ vector $(-c_2, c_1^*)^T$. This gives the Néel magnetic order momentum,

$$\mathbf{S}(\mathbf{r}) = (-1)^{\mathbf{r}} \mathbf{n}. \quad (\text{C8})$$

Appendix D: Magnetic order from the π -flux state

In the large κ limit, the spinon in the π -flux spin liquid phase will also condense and form magnetic order. In this section, we discuss the magnetic order from the π -flux state.

The mean-field Hamiltonian of (π, π) -flux state is

$$H_{\text{MF}} = \sum_{\mathbf{k}} \Psi_{\mathbf{k}}^\dagger D_{\mathbf{k}} \Psi_{\mathbf{k}} + N_s \left[\mu + \mu\kappa + 8J_1(|A_1|^2 - |B_1|^2) + 2J_2|A_2|^2 \right], \quad (\text{D1})$$

where the expression $D_{\mathbf{k}}$ is shown in Eq. (B29).

For simplicity, we only discuss the large J_1 condition, where only A_1 is finite. In the mean-field level, the Shastry-Sutherland lattice is equivalent to the square lattice in this condition where A_2 and B_2 vanishes. The magnetic order of this condition is

$$\mathbf{S}(X, Y, 0) = \mathbf{n}_1 + \mathbf{n}_2 + \mathbf{n}_3, \quad (\text{D2})$$

$$\mathbf{S}(X, Y, 1) = -\mathbf{n}_1 + \mathbf{n}_2 - \mathbf{n}_3, \quad (\text{D3})$$

$$\mathbf{S}(X, Y, 2) = -\mathbf{n}_1 + \mathbf{n}_2 + \mathbf{n}_3, \quad (\text{D4})$$

$$\mathbf{S}(X, Y, 3) = \mathbf{n}_1 + \mathbf{n}_2 - \mathbf{n}_3, \quad (\text{D5})$$

which is discussed in Ref. [37], and $n_1^2 + n_2^2 + n_3^2 = n^2$. The details of the calculation can be referred to Appendix C in Ref. [37].

Appendix E: Self-consistent spin wave theory

In this section, we introduce the self-consistent spin wave theory in details. Near the phase boundary of the Néel phase, the quantum fluctuation is significant and the interaction of magnons takes important role. For the Shastry-Sutherland model, the linear spin wave Hamiltonian is not positive or semi-positive definite in $J_1/J_2 < 1$, and the linear spin wave theory breaks down in this region. The nonlinear spin wave theory also breaks down because the correction of magnon interaction depends on the magnon wave function of linear spin wave theory. Therefore, we need to use a self-consistent spin wave theory to study Néel phase of the Shastry-Sutherland model in $J_1/J_2 < 1$.

Spin wave theory is to describe the ordered phase in terms of small fluctuations of the spins about their expectation values, which can be regarded as the classical ground state of the Hamiltonian. For the Shastry-Sutherland model, the magnetic ordered state is a Néel state, and the classical ground state is the Néel antiferromagnetic state. With the classical ground state, the spin Hamiltonian can be expressed by the boson operators by the Holstein-Primakoff transformation[38]. Expanding the Hamiltonian by $1/S$ as we regarding S as a large number, the Hamiltonian is transformed to

$$H = H_0 + H_2 + H_4 + H_6 + \dots, \quad (\text{E1})$$

where linear term H_1 vanishes if the classical ground state is proper. Keeping up to quadratic terms H_2 , one obtains the noninteracting spin wave Hamiltonian. The higher order terms $H_4 + H_6 + \dots$ introduce the interactions of magnons. For the Shastry-Sutherland model, if we choose the “ J_2 -square” as the unit cell, the linear spin wave Hamiltonian H_2 in the momentum space can be written as

$$H_2 = \sum_{\mathbf{k}} \left(a_{\mathbf{k}}^\dagger \ b_{\mathbf{k}}^\dagger \ c_{\mathbf{k}}^\dagger \ d_{\mathbf{k}}^\dagger \ a_{-\mathbf{k}} \ b_{-\mathbf{k}} \ c_{-\mathbf{k}} \ d_{-\mathbf{k}} \right) \mathcal{H}_{\mathbf{k}} \begin{pmatrix} a_{\mathbf{k}} \\ b_{\mathbf{k}} \\ c_{\mathbf{k}} \\ d_{\mathbf{k}} \\ a_{-\mathbf{k}}^\dagger \\ b_{-\mathbf{k}}^\dagger \\ c_{-\mathbf{k}}^\dagger \\ d_{-\mathbf{k}}^\dagger \end{pmatrix}, \quad (\text{E2})$$

here a, b, c, d are the Holstein-Primakoff bosons for the unit cell has 4 sites. The $\mathcal{H}_{\mathbf{k}}$ satisfies

$$\mathcal{H}_{\mathbf{k}} = \begin{pmatrix} \mathbf{B}_{\mathbf{k}} & \mathbf{A}_{\mathbf{k}} \\ \mathbf{A}_{\mathbf{k}}^\dagger & \mathbf{B}_{-\mathbf{k}}^T \end{pmatrix}, \quad (\text{E3})$$

$$\mathbf{A}_{\mathbf{k}} = \begin{pmatrix} 0 & \frac{1}{2}J_1(1 + e^{ik_1}) & 0 & \frac{1}{2}J_1(1 + e^{ik_2}) \\ \frac{1}{2}J_1(1 + e^{-ik_1}) & 0 & \frac{1}{2}J_1(1 + e^{ik_2}) & 0 \\ 0 & \frac{1}{2}J_1(1 + e^{-ik_2}) & 0 & \frac{1}{2}J_1(1 + e^{-ik_1}) \\ \frac{1}{2}J_1(1 + e^{-ik_2}) & 0 & \frac{1}{2}J_1(1 + e^{ik_1}) & 0 \end{pmatrix}, \quad (\text{E4})$$

$$\mathbf{B}_{\mathbf{k}} = \begin{pmatrix} 2J_1 - \frac{1}{2}J_2 & 0 & 0 & 0 \\ 0 & 2J_1 - \frac{1}{2}J_2 & 0 & \frac{1}{2}J_2 e^{i(k_1 - k_2)} \\ 0 & 0 & 2J_1 - \frac{1}{2}J_2 & 0 \\ 0 & \frac{1}{2}J_2 e^{i(-k_1 + k_2)} & 0 & 2J_1 - \frac{1}{2}J_2 \end{pmatrix}. \quad (\text{E5})$$

Using Bogoliubov transformation to diagonalize the $\mathcal{H}_{\mathbf{k}}$, we will get the linear spin wave dispersion and wave functions, which breaks down at $J_1/J_2 < 1$. The self-consistent spin wave theory is to use the boson-pair expectation values to decouple the quartic terms. We use a specific term for example:

$$\begin{aligned} & \sum_{\mathbf{k}, \mathbf{p}, \mathbf{q}} V(\mathbf{k}, \mathbf{p}, \mathbf{q}) a_{\mathbf{k}}^\dagger b_{\mathbf{p}}^\dagger a_{\mathbf{q}} b_{\mathbf{k}+\mathbf{p}-\mathbf{q}} \\ & \approx \sum_{\mathbf{k}} \left[\sum_{\mathbf{p}, \mathbf{q}} V(\mathbf{k}, \mathbf{p}, \mathbf{k}) \langle b_{\mathbf{p}}^\dagger b_{\mathbf{p}} \rangle \right] a_{\mathbf{k}}^\dagger a_{\mathbf{k}} + \dots \\ & = \sum_{\mathbf{k}} f(\mathbf{k}) a_{\mathbf{k}}^\dagger a_{\mathbf{k}} + \dots \end{aligned} \quad (\text{E6})$$

Here a and b are the boson operators of different flavors, and we set $\sum_{\mathbf{k}} f(\mathbf{k}) \equiv \sum_{\mathbf{p}, \mathbf{q}} V(\mathbf{k}, \mathbf{p}, \mathbf{k}) \langle b_{\mathbf{p}}^\dagger b_{\mathbf{p}} \rangle$. The symbol (...) represents the other decoupling types. Therefore, the Hamiltonian is transformed into

$$\begin{aligned} H &= H_2 + H_4 + \dots \\ &= H_2 + \tilde{H}_2 + H_4 - \tilde{H}_2 + \dots \\ &= H'_2 + H'_4, \end{aligned} \quad (\text{E7})$$

and $H'_4 = 0$ in the mean-field level. We call this theory a self-consistent spin wave theory because the decoupled quartic term \tilde{H}_2 need to be calculated self-consistently. The effects of magnon interaction is considered in this theory. When H_2 is not positive or semi-positive definite, this method may also work because we only need to keep H'_2 to be positive and semi-positive definite. For the Shastry-Sutherland model, the self-consistent spin wave theory works in the $J_1/J_2 > 0.65$, where the magnetic order parameter vanishes, which indicates the phase boundary of the Néel state.

Appendix F: Continuum limit of linear spin wave on Shastry-Sutherland model

In this section, we follow the prescription in Refs. [39] to derive the continuum field theory of the linear spin wave on Shastry-Sutherland model. The magnon velocity can be obtained from this continuum field theory.

We assume the Néel order is along the z direction

$$\langle \mathbf{S}_i \rangle = (-1)^s S \hat{\mathbf{z}}, \quad (\text{F1})$$

here $s = 0, 1, 2, 3$, which is the sublattice label shown in Fig. 6. The lattice vectors are $2\hat{\mathbf{x}}$ and $2\hat{\mathbf{y}}$. The site position in the Shastry-Sutherland lattice is expressed by (\mathbf{r}, s) , where \mathbf{r} is the unit cell position and s is the sublattice label. After Holstein-Primakoff transformation, the linear spin wave Hamiltonian is

$$\begin{aligned} H_{LSW} = S \sum_{\mathbf{r}} & \left\{ (4J_1 - J_2) \sum_s b_{s\mathbf{r}}^\dagger b_{s\mathbf{r}} + J_2 \left(b_{1\mathbf{r}}^\dagger b_{3\mathbf{r}+\hat{\mathbf{x}}+\hat{\mathbf{y}}} + b_{0\mathbf{r}}^\dagger b_{2\mathbf{r}+\hat{\mathbf{x}}-\hat{\mathbf{y}}} + \text{h.c.} \right) \right. \\ & \left. - J_1 [b_{0\mathbf{r}} (b_{1\mathbf{r}+\hat{\mathbf{x}}} + b_{1\mathbf{r}-\hat{\mathbf{x}}} + b_{3\mathbf{r}+\hat{\mathbf{y}}} + b_{3\mathbf{r}-\hat{\mathbf{y}}}) + b_{2\mathbf{r}} (b_{1\mathbf{r}+\hat{\mathbf{y}}} + b_{1\mathbf{r}-\hat{\mathbf{y}}} + b_{3\mathbf{r}+\hat{\mathbf{x}}} + b_{3\mathbf{r}-\hat{\mathbf{x}}}) + \text{h.c.}] \right\}. \end{aligned} \quad (\text{F2})$$

In the imaginary time path integral formalism, the bosonic $b_{s\mathbf{r}}$ operators become complex fields. For later convenience, the operators are transformed to complex fields as

$$b_{0\mathbf{r}} \rightarrow \phi_0(\mathbf{r}), \quad (\text{F3})$$

$$b_{1\mathbf{r}} \rightarrow \phi_1^*(\mathbf{r}), \quad (\text{F4})$$

$$b_{2\mathbf{r}} \rightarrow \phi_2(\mathbf{r}), \quad (\text{F5})$$

$$b_{3\mathbf{r}} \rightarrow \phi_3^*(\mathbf{r}). \quad (\text{F6})$$

The gradient expansion is used to get the continuum field theory from the linear spin wave Hamiltonian in Eq. (F2),

$$\phi_s^*(\mathbf{r})\phi_{s'}(\mathbf{r} + \mathbf{a}) = \phi_s^*(\mathbf{r}) \left[\phi_{s'}(\mathbf{r}) + \mathbf{a} \cdot \nabla_{\mathbf{r}} \phi_{s'}(\mathbf{r}) + \frac{1}{2} (\mathbf{a} \cdot \nabla_{\mathbf{r}})^2 \phi_{s'}(\mathbf{r}) + \dots \right]. \quad (\text{F7})$$

Substituting the gradient expansion to the linear spin wave Hamiltonian and keep up to the 2nd order, we obtains the Hamiltonian density,

$$\mathcal{H} = \mathcal{H}_0 + \mathcal{H}_1 + \mathcal{H}_2, \quad (\text{F8})$$

here \mathcal{H}_0 has no gradient, \mathcal{H}_1 has the 1st order gradient terms and \mathcal{H}_2 has the 2st order gradient terms. The expression of \mathcal{H}_0 is

$$\mathcal{H}_0 = \begin{pmatrix} \phi_0^*(\mathbf{r}) & \phi_1^*(\mathbf{r}) & \phi_2^*(\mathbf{r}) & \phi_3^*(\mathbf{r}) \end{pmatrix} \begin{pmatrix} 4J_1 - J_2 & -2J_1 & J_2 & -2J_1 \\ -2J_1 & 4J_1 - J_2 & -2J_1 & J_2 \\ J_2 & -2J_1 & 4J_1 - J_2 & -2J_1 \\ -2J_1 & J_2 & -2J_1 & 4J_1 - J_2 \end{pmatrix} \begin{pmatrix} \phi_0(\mathbf{r}) \\ \phi_1(\mathbf{r}) \\ \phi_2(\mathbf{r}) \\ \phi_3(\mathbf{r}) \end{pmatrix}, \quad (\text{F9})$$

and the eigenvalues and eigenvectors of \mathcal{H}_0 are

$$0, \Psi_0 = \begin{pmatrix} 1/2 \\ 1/2 \\ 1/2 \\ 1/2 \end{pmatrix}; 8J_1 S, \Psi_1 = \begin{pmatrix} 1/2 \\ -1/2 \\ 1/2 \\ -1/2 \end{pmatrix}; (4J_1 - 2J_2)S, \Psi_2 = \begin{pmatrix} 1/2 \\ 1/2 \\ -1/2 \\ -1/2 \end{pmatrix}; (4J_1 - 2J_2)S, \Psi_3 = \begin{pmatrix} 1/2 \\ -1/2 \\ -1/2 \\ 1/2 \end{pmatrix}; \quad (\text{F10})$$

The eigenvector Ψ_0 with zero eigenvalue is the Goldstone mode. Then the \mathcal{H}_0 is diagonalized as

$$\mathcal{H}_0 = 8SJ_1 \Psi_1^* \Psi_1 + S(4J_1 - 2J_2)(\Psi_2^* \Psi_2 + \Psi_3^* \Psi_3). \quad (\text{F11})$$

For later convenience, we set $\phi \equiv (\phi_0(\mathbf{r}) \ \phi_1(\mathbf{r}) \ \phi_2(\mathbf{r}) \ \phi_3(\mathbf{r}))^T$ and $\Psi \equiv (\Psi_0(\mathbf{r}) \ \Psi_1(\mathbf{r}) \ \Psi_2(\mathbf{r}) \ \Psi_3(\mathbf{r}))^T$. The expression of \mathcal{H}_1 is

$$\begin{aligned} \mathcal{H}_1 &= SJ_2[\phi_1(\partial_x + \partial_y)\phi_3^* + \phi_0^*(\partial_x - \partial_y)\phi_2 - \phi_3(\partial_x + \partial_y)\phi_1^* - \phi_2^*(\partial_x - \partial_y)\phi_0] \\ &= SJ_2 \left[\phi^* \begin{pmatrix} 0 & 0 & 1 & 0 \\ 0 & 0 & 0 & 1 \\ -1 & 0 & 0 & 0 \\ 0 & -1 & 0 & 0 \end{pmatrix} \partial_x \phi + \phi^* \begin{pmatrix} 0 & 0 & -1 & 0 \\ 0 & 0 & 0 & 1 \\ 1 & 0 & 0 & 0 \\ 0 & -1 & 0 & 0 \end{pmatrix} \partial_y \phi \right] \\ &= SJ_2 \left[\Psi^* \begin{pmatrix} 0 & 0 & -1 & 0 \\ 0 & 0 & 0 & -1 \\ 1 & 0 & 0 & 0 \\ 0 & 1 & 0 & 0 \end{pmatrix} \partial_x \Psi + \Psi^* \begin{pmatrix} 0 & 0 & 0 & -1 \\ 0 & 0 & -1 & 0 \\ 0 & 1 & 0 & 0 \\ 1 & 0 & 0 & 0 \end{pmatrix} \partial_y \Psi \right]. \quad (\text{F12}) \end{aligned}$$

Now we consider the 2nd order gradient terms \mathcal{H}_2 , whose expression is

$$\begin{aligned} \mathcal{H}_2 &= \frac{1}{2} SJ_2[\phi_1(\partial_x + \partial_y)^2 \phi_3^* + \phi_0(\partial_x - \partial_y)^2 \phi_2^* + \phi_3(\partial_x + \partial_y)^2 \phi_1^* + \phi_2(\partial_x - \partial_y)^2 \phi_0^*] \\ &\quad - SJ_1[\phi_0(\partial_x^2 \phi_1^* + \partial_y^2 \phi_3^*) + \phi_2(\partial_y^2 \phi_1^* + \partial_x^2 \phi_3^*) + \text{c.c.}]. \quad (\text{F13}) \end{aligned}$$

In the continuum limit, the low energy effective theory is only contributed by the Goldstone mode Ψ_0 . Therefore, we need to integrate the high energy modes Ψ_1, Ψ_2 and Ψ_3 to get the effective field theory of Ψ_0 . For this purpose, we only keep the $\Psi_0^*(\dots)\Psi_0$ terms in \mathcal{H}_2 because the other terms in \mathcal{H}_2 do not contribute the effective field theory of Ψ_0 up to 2nd order gradient terms. Then we just need to replace ϕ_s by $\frac{1}{2}\Psi_0$,

$$\begin{aligned} \mathcal{H}_2 &\cong \frac{1}{4} SJ_2[\Psi_0(\partial_x + \partial_y)^2 \Psi_0^* + \Psi_0(\partial_x - \partial_y)^2 \Psi_0^*] - \frac{1}{2} SJ_1[\Psi_0(\partial_x^2 + \partial_y^2) \Psi_0^* + \Psi_0^*(\partial_x^2 + \partial_y^2) \Psi_0] + \dots \\ &= S(J_1 - \frac{1}{2}J_2) [(\partial_x \Psi_0^*)(\partial_x \Psi_0) + (\partial_y \Psi_0^*)(\partial_y \Psi_0)]. \quad (\text{F14}) \end{aligned}$$

The Lagrangian density of the linear spin wave theory is

$$\begin{aligned} \mathcal{L} &= \phi_0^* \partial_\tau \phi_0 - \phi_1^* \partial_\tau \phi_1 + \phi_2^* \partial_\tau \phi_2 - \phi_3^* \partial_\tau \phi_3 - \mathcal{H} \\ &= \Psi_0^* \partial_\tau \Psi_1 + \Psi_1^* \partial_\tau \Psi_0 + \Psi_2^* \partial_\tau \Psi_3 + \Psi_3^* \partial_\tau \Psi_2 - \mathcal{H}. \quad (\text{F15}) \end{aligned}$$

J_1/J_2	0.7	0.75	0.8	0.85	0.9	0.95	1	1.05	1.1	1.15	1.2	1.25	1.13	1.35	1.4
v_{SCSW}	0.470	0.585	0.695	0.802	0.905	1.005	1.103	1.199	1.294	1.387	1.478	1.569	1.659	1.748	1.836
v_{LSW}	n.a.	n.a.	n.a.	n.a.	n.a.	n.a.	0	0.447	0.635	0.781	0.907	1.021	1.126	1.225	1.320
m_{SCSW}	0.032	0.069	0.096	0.116	0.130	0.143	0.153	0.160	0.166	0.171	0.176	0.180	0.183	0.186	0.188
m_{LSW}	n.a.	0.067	0.109	0.136	0.156	0.171	0.183	0.193							

TABLE I: Magnon velocities and magnetic moment sizes from self-consistent spin wave(SCSW) and linear spin wave(LSW). The unit of the velocities is $J_2 a$, where a is the square lattice constant. The magnetic moment is calculated by $1/2 - \langle n_m \rangle$, here $\langle n_m \rangle$ is the average magnon density. “n.a.” means not applicable.

By integrating the high energy modes by Gaussian part of their action in \mathcal{H} , we get the effective action for Ψ_0 , whose Lagrangian density is

$$\mathcal{L}_{\text{eff}} = \frac{1}{8SJ_1} (\partial_\tau \Psi_0^*) (\partial_\tau \Psi_0) + S \left[J_1 - \frac{J_2}{2} - \frac{J_2^2}{4J_1 - 2J_2} \right] [(\partial_x \Psi_0^*) (\partial_x \Psi_0) + (\partial_y \Psi_0^*) (\partial_y \Psi_0)], \quad (\text{F16})$$

which yields the dispersion relation

$$\frac{1}{8SJ_1} \omega^2 = S \left[J_1 - \frac{J_2}{2} - \frac{J_2^2}{4J_1 - 2J_2} \right] \mathbf{k}^2. \quad (\text{F17})$$

Finally, we get the magnon velocity v_{sw} of linear spin wave theory,

$$v_{\text{sw}} = 4SJ_1 \sqrt{\frac{J_1 - J_2}{2J_1 - J_2}}, \quad (\text{F18})$$

which vanishes at $J_1 = J_2$, where the linear spin wave theory breaks down. For the magnon velocity of the self-consistent spin wave theory, it can only be calculated numerically. The magnon velocities and magnetic moment sizes calculated by self-consistent and linear spin wave theory are shown in Table I.

Appendix G: Exact diagonalization of 32-site Shastry-Sutherland model

We study the ground state properties of the Shastry-Sutherland model [see Eq. (1) in Main Text] by exact diagonalization, on finite-size($2\sqrt{2} \times 2\sqrt{2} \times 4$) lattice with 32 sites (see Fig. 18). With periodic boundary conditions this preserves the full lattice symmetries of the Shastry-Sutherland model.

The ground state energies and wave functions are obtained by the Lanczos method. The following lattice symmetries are exploited to reduce the Hilbert space sizes, (a) lattice translations (with respect to 4-site unit cell); (b) four-fold rotation C_4 around the center of an empty square, in the translation trivial sector. The ground states are found in the sector with trivial translations and C_4 eigenvalue (+1). The reduced Hilbert space sizes is 18788230 for this 32-site lattice.

We consider antiferromagnetic J_1 and J_2 couplings and set $J_2 = 1$. The ground state energy and some of the ground state spin-spin correlation functions are shown in Fig. 4 in Main Text. We note that for $J_1/J_2 \leq 0.67578125$ the exact ground state is the dimer-singlet state, and a level crossing happens for J_1/J_2 between 0.67578125 and 0.677734375. This level crossing point is consistent with previous exact diagonalization studies [25]

Here we also present the ground state expectation values of the 4-site ring exchange operators around “ J_2 square” and “empty square” from the exact diagonalization, and compare them to the Schwinger boson mean-field theory results (see Fig. 19). This operator cyclically permutes spins on the four sites involved, namely it is $\sum_{\{s_i\}} (|s_1, s_2, s_3, s_4\rangle \langle s_2, s_3, s_4, s_1| + \text{h.c.})$.

-
- [1] Y. Cui, L. Liu, H. Lin, K.-H. Wu, W. Hong, X. Liu, C. Li, Z. Hu, N. Xi, S. Li, R. Yu, A. W. Sandvik, and W. Yu, Proximate deconfined quantum critical point in $\text{srcu}_2(\text{bo}_3)_2$, *Science* **380**, 1179 (2023), <https://www.science.org/doi/pdf/10.1126/science.adc9487>.
- [2] M. E. Zayed, C. Rüegg, J. Larrea J., A. M. Läuchli, C. Panagopoulos, S. S. Saxena, M. Ellerby, D. F. McMorrow, T. Strässle, S. Klotz, G. Hamel, R. A. Sadykov, V. Pomjakushin, M. Boehm, M. Jiménez-Ruiz, A. Schneidewind, E. Pomjakushina, M. Stingaciu, K. Conder, and H. M. Rønnow, 4-spin plaquette singlet state in the shastry-sutherland compound $\text{srcu}_2(\text{bo}_3)_2$, *Nature Physics* **13**, 962 (2017).

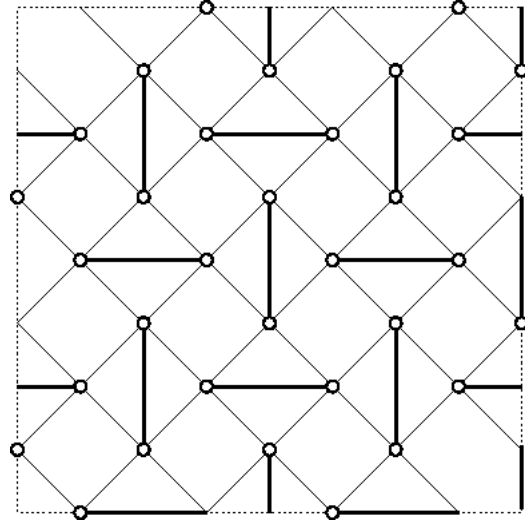


FIG. 18: The 32-site Shastry-Sutherland lattice used in the ED study. Open circles indicate distinct sites under periodic boundary condition. J_2 and J_1 bonds are depicted as thick and thin solid lines respectively.

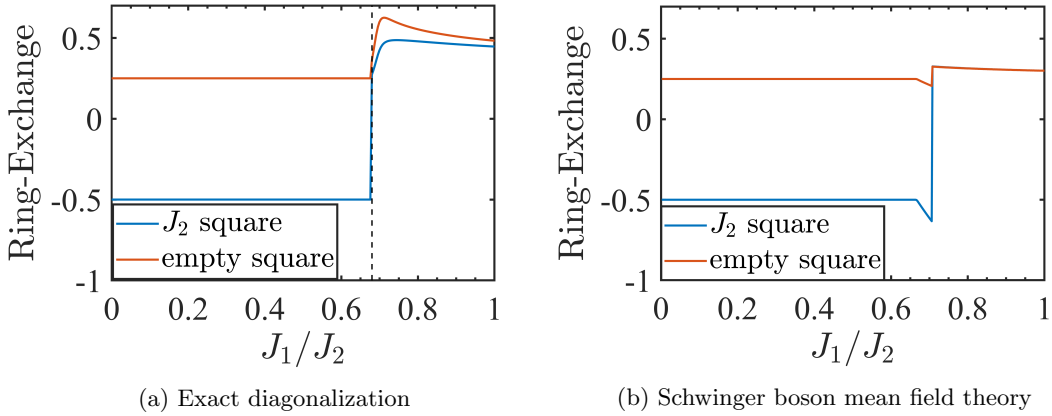


FIG. 19: Expectation values of 4-site ring exchange operators around “ J_2 square” and “empty square” calculated by (a) exact diagonalization and (b) Schwinger boson mean field theory.

- [3] J. Guo, G. Sun, B. Zhao, L. Wang, W. Hong, V. A. Sidorov, N. Ma, Q. Wu, S. Li, Z. Y. Meng, A. W. Sandvik, and L. Sun, Quantum phases of $\text{srcu}_2(\text{bo}_3)_2$ from high-pressure thermodynamics, *Phys. Rev. Lett.* **124**, 206602 (2020).
- [4] J. L. Jiménez, S. P. G. Crone, E. Fogh, M. E. Zayed, R. Lortz, E. Pomjakushina, K. Conder, A. M. Läuchli, L. Weber, S. Wessel, A. Honecker, B. Normand, C. Rüegg, P. Corboz, H. M. Rønnow, and F. Mila, A quantum magnetic analogue to the critical point of water, *Nature* **592**, 370 (2021).
- [5] T. Senthil, A. Vishwanath, L. Balents, S. Sachdev, and M. P. A. Fisher, Deconfined quantum critical points, *Science* **303**, 1490 (2004), <https://www.science.org/doi/pdf/10.1126/science.1091806>.
- [6] S. Sachdev, Quantum magnetism and criticality, *Nature Physics* **4**, 173 (2008).
- [7] A. W. Sandvik, Evidence for deconfined quantum criticality in a two-dimensional heisenberg model with four-spin interactions, *Phys. Rev. Lett.* **98**, 227202 (2007).
- [8] N. Xi, H. Chen, Z. Y. Xie, and R. Yu, Plaquette valence bond solid to antiferromagnet transition and deconfined quantum critical point of the shastry-sutherland model, *Phys. Rev. B* **107**, L220408 (2023).
- [9] L. Balents, Spin liquids in frustrated magnets, *Nature* **464**, 199 (2010).
- [10] B. Sriram Shastry and B. Sutherland, Exact ground state of a quantum mechanical antiferromagnet, *Physica B+C* **108**, 1069 (1981).
- [11] H. Nakano and T. Sakai, Third boundary of the shastry-sutherland model by numerical diagonalization, *Journal of the Physical Society of Japan* **87**, 123702 (2018), <https://doi.org/10.7566/JPSJ.87.123702>.
- [12] A. Koga and N. Kawakami, Quantum phase transitions in the shastry-sutherland model for $\text{srcu}_2(\text{bo}_3)_2$, *Phys. Rev. Lett.* **84**, 4461 (2000).

- [13] B. Zhao, P. Weinberg, and A. W. Sandvik, Symmetry-enhanced discontinuous phase transition in a two-dimensional quantum magnet, *Nature Physics* **15**, 678 (2019).
- [14] P. Corboz and F. Mila, Tensor network study of the shastry-sutherland model in zero magnetic field, *Phys. Rev. B* **87**, 115144 (2013).
- [15] Z. Weihong, C. J. Hamer, and J. Oitmaa, Series expansions for a heisenberg antiferromagnetic model for $\text{SrCu}_2(\text{BO}_3)_2$, *Phys. Rev. B* **60**, 6608 (1999).
- [16] Y. Takushima, A. Koga, and N. Kawakami, Competing spin-gap phases in a frustrated quantum spin system in two dimensions, *Journal of the Physical Society of Japan* **70**, 1369 (2001), <https://doi.org/10.1143/JPSJ.70.1369>.
- [17] Albrecht, M. and Mila, F., First-order transition between magnetic order and valence bond order in a 2d frustrated heisenberg model, *Europhys. Lett.* **34**, 145 (1996).
- [18] S. Miyahara and K. Ueda, Theory of the orthogonal dimer heisenberg spin model for $\text{SrCu}_2(\text{BO}_3)_2$, *Journal of Physics: Condensed Matter* **15**, R327 (2003).
- [19] W. Zheng, J. Oitmaa, and C. J. Hamer, Phase diagram of the shastry-sutherland antiferromagnet, *Phys. Rev. B* **65**, 014408 (2001).
- [20] J. Y. Lee, Y.-Z. You, S. Sachdev, and A. Vishwanath, Signatures of a deconfined phase transition on the shastry-sutherland lattice: Applications to quantum critical $\text{SrCu}_2(\text{BO}_3)_2$, *Phys. Rev. X* **9**, 041037 (2019).
- [21] A. Läuchli, S. Wessel, and M. Sgrist, Phase diagram of the quadrumerized shastry-sutherland model, *Phys. Rev. B* **66**, 014401 (2002).
- [22] C. Boos, S. P. G. Crone, I. A. Niesen, P. Corboz, K. P. Schmidt, and F. Mila, Competition between intermediate plaquette phases in $\text{SrCu}_2(\text{BO}_3)_2$ under pressure, *Phys. Rev. B* **100**, 140413 (2019).
- [23] J. Wang, H. Li, N. Xi, Y. Gao, Q.-B. Yan, W. Li, and G. Su, Plaquette singlet transition, magnetic barocaloric effect, and spin supersolidity in the shastry-sutherland model (2023), [arXiv:2302.06596 \[cond-mat.str-el\]](https://arxiv.org/abs/2302.06596).
- [24] J. Yang, A. W. Sandvik, and L. Wang, Quantum criticality and spin liquid phase in the shastry-sutherland model, *Phys. Rev. B* **105**, L060409 (2022).
- [25] L. Wang, Y. Zhang, and A. W. Sandvik, Quantum spin liquid phase in the shastry-sutherland model detected by an improved level spectroscopic method, *Chinese Physics Letters* **39**, 077502 (2022).
- [26] A. Keleş and E. Zhao, Rise and fall of plaquette order in the shastry-sutherland magnet revealed by pseudofermion functional renormalization group, *Phys. Rev. B* **105**, L041115 (2022).
- [27] Y. Zhou, K. Kanoda, and T.-K. Ng, Quantum spin liquid states, *Rev. Mod. Phys.* **89**, 025003 (2017).
- [28] S. Sachdev, Kagomé- and triangular-lattice heisenberg antiferromagnets: Ordering from quantum fluctuations and quantum-disordered ground states with unconfined bosonic spinons, *Phys. Rev. B* **45**, 12377 (1992).
- [29] S. Sachdev, Kagomé- and triangular-lattice heisenberg antiferromagnets: Ordering from quantum fluctuations and quantum-disordered ground states with unconfined bosonic spinons, *Phys. Rev. B* **45**, 12377 (1992).
- [30] X.-G. Wen, Quantum orders and symmetric spin liquids, *Phys. Rev. B* **65**, 165113 (2002).
- [31] F. Wang and A. Vishwanath, Spin-liquid states on the triangular and kagomé lattices: A projective-symmetry-group analysis of schwinger boson states, *Phys. Rev. B* **74**, 174423 (2006).
- [32] A. Polyakov, Quark confinement and topology of gauge theories, *Nuclear Physics B* **120**, 429 (1977).
- [33] J. Takano, H. Tsunetsugu, and M. E. Zhitomirsky, Self-consistent spin wave analysis of the magnetization plateau in triangular antiferromagnet, *Journal of Physics: Conference Series* **320**, 012011 (2011).
- [34] V. V. Mkhitarian and L. Ke, Self-consistently renormalized spin-wave theory of layered ferromagnets on the honeycomb lattice, *Phys. Rev. B* **104**, 064435 (2021).
- [35] H. Nakano and T. Sakai, Large-scale numerical-diagonalization study of the shastry-sutherland model (Journal of the Physical Society of Japan, 2023) 0.
- [36] A. M. Essin and M. Hermele, Classifying fractionalization: Symmetry classification of gapped F_2 spin liquids in two dimensions, *Phys. Rev. B* **87**, 104406 (2013).
- [37] X. Yang and F. Wang, Schwinger boson spin-liquid states on square lattice, *Phys. Rev. B* **94**, 035160 (2016).
- [38] T. Holstein and H. Primakoff, Field dependence of the intrinsic domain magnetization of a ferromagnet, *Phys. Rev.* **58**, 1098 (1940).
- [39] S. Sachdev, Quantum phase transitions of antiferromagnets and the cuprate superconductors, in *Modern Theories of Many-Particle Systems in Condensed Matter Physics*, edited by D. C. Cabra, A. Honecker, and P. Pujol (Springer Berlin Heidelberg, Berlin, Heidelberg, 2012) pp. 1–51.